Charles University
Faculty of Science

Study programme: Chemistry
Branch of study: Biophysical Chemistry

Bc. Jana Nedvědová

Analysis of Histone Deacetylase 6/Kinesin Interactions

Popis interakcí mezi histondeacetylasou 6 a kinesinem

Diploma thesis

Supervisor: RNDr. Cyril Bařinka, PhD.

Prague, 2019

Prohlášení

Prohlašuji, že jsem závěrečnou práci zpracoval/a samostatně a že jsem uvedl/a všechny použité informační zdroje a literaturu. Tato práce ani její podstatná část nebyla předložena k získání jiného nebo stejného akademického titulu.

V Praze dne 3. května 2019 Jana Nedvědová

.....

Acknowledgements

In the first place, I would like to thank to Cyril Bařinka for the ongoing opportunity to work in his lab and the time he spent discussing my results and correcting my writing. I also thank to him and all the other members of our lab, namely Kuba, Bára, velká Jana, Kseniya, Zsofka, Zorka, Shivam, Petra, Iva, Markéta and Gargi, for creating friendly working environment and great teambuilding activities. I thank one more time to Zorka for teaching me how to do HDX experiments, Bára for her help with cloning and Kuba for trying to find answers to my never-ending questions.

I thank to my friends Karol and Ráchel for being there for me and bearing my existence especially in the last months of my studies. In the last place, I thank to my parents for their support for the whole five years at university.

Abstract

Intracellular transport is provided by two major types of molecular motors kinesins and cytoplasmic dynein. Kinesin-1 is a molecular motor that transports molecules and organelles along microtubule tracks anterogradely. Specific protein-protein interactions are required to activate kinesin-1 as the free kinesin exist in an autoinhibited state. The activation of kinesin-1 induces its conformational change, enables microtubule binding and ATP hydrolysis necessary for the directional cargo transport.

HDAC6 is a multifunctional protein composed of several domains. It plays an important role in many microtubule dependent processes as HDAC6 is a major tubulin deacetylase. It has been shown that HDAC6 manipulation (inhibition/genetic ablation) affects transport along microtubules but the exact mechanisms are unknown. The effect can be caused either by deacetylation microtubules or direct interaction with molecular motors.

This thesis is focused on characterization of interactions between kinesin-1 and HDAC6 that have not been described so far. To this end, we expressed and purified various constructs of kinesin-1 and HDAC6 and tested their interactions by microscale thermophoresis (MST) and hydrogen deuterium exchange (HDX) to determine affinity and interaction sites, respectively. MST data revealed that HDAC6 interacts with kinesin-1 with high nanomolar affinity and the C-terminal part of kinesin-1 is responsible for the interaction. HDX results confirmed that the C-terminal part kinesin-1 is the predominant interaction interface and the deacetylase domain 2 of HDAC6 was shown to be mainly responsible for the interaction with kinesin-1.

Key words: histone deacetylase 6, HDAC6, kinesin-1, KIF5B, protein-protein interactions, hydrogen/deuterium exchange, microscale thermophoresis

Abstrakt

Intracelulární transport je zajišťován dvěma typy molekulárních motorů, kinesiny a dyneiny. Kinesin-1 zprostředkovává transport molekul and organel podél mikrotubulů směrem k jejich plus konci. Specifické protein-proteinové interakce jsou nezbytné k aktivaci kinesinu, protože volný kinesin je autoinhibován. Aktivace kinesinu je spojena se změnou jeho konformace. Aktivovaný kinesin se váže na mikrotubuly a za hydrolýzy ATP přenáší navázané molekuly a organely.

HDAC6 je multifunkční protein složený z několika domén. Je důležitým regulačním faktorem v mnoha procesech týkajících se mikrotubulů. HDAC6 je totiž hlavním enzymem deacetylujícím mikrotubuly. Bylo popsáno, že inaktivace HDAC6 ovlivňuje transport na mikrotubulech, nicméně mechanismus těchto změn není znám. Inaktivace HDAC6 může tyto změny působit kvůli posttranslační modifikaci mikrotubulů nebo přímou interakcí s molekulárními motory.

Tato diplomová práce je zaměřena na charakterizaci dosud nepopsané interakce mezi kinesinem-1 a HDAC6. Za tímto účelem byla provedena exprese a purifikace navržených konstruktů obou proteinů. Tyto konstrukty byly analyzovány pomocí mikroskopické termoforézy (MST) pro stanovení jejich vzájemné afinity a vodík-deuteriové výměny (HDX), kterou byly interakce popsány ze strukturního hlediska. Podle MST je afinita mezi kinesinem-1 a HDAC6 submikromolární. HDX experimenty potvrzují, že C-terminální část kinesinu je zodpovědná za interakci s HDAC6. HDAC6 obsahuje dvě deacetylasové domény, za interakci s kinesinem-1 je zodpovědná druhá z nich.

Klíčová slova: histondeacetylasa 6, HDAC6, kinesin-1, KIF5B, protein-proteinové interakce, H/D výměna, thermoforéza

List of Abbreviations

AA	Amino acids
ApoER2	Apolipoprotein E receptor 2
APP	Amyloid precursor protein
APS	Ammonium persulfate
bp	Base pairs
drHDAC6	Danio rerio HDAC6
DSG	Disuccinimidyl glutarate
DSS	Disuccinimidyl suberate
EDAC	1-Ethyl-3-(3-dimethylaminopropyl)carbodiimide
EDTA	Ethylenediaminetetraacetic acid
FEZ1	Fasciculation and elongation protein zeta-1
FPLC	Fast protein liquid chromatography
GDP	Guanosine diphosphate
GFP	Green fluorescent protein
GRIP1	Glutamate receptor-interacting protein
GTP	Guanosine triphosphate
HDAC	Histone deacetylase
HDX	Hydrogen/deuterium exchange
hHDAC6	Human HDAC6
IDP	Intrinsically disordered protein
JIP	JNK interacting protein
JNK	c-Jun N-terminal kinase
KAT	Lysine acetyltransferase
KDAC	Lysine deacetylase
LC	Liquid chromatography
MAPK	Mitogen-activated protein kinase
MS	Mass spectrometry
MST	Microscale thermophoresis
NAT	N-terminus acetyltransferase
NiNTA	Nickel(II)-Nitrilotriacetic acid
PAGE	Polyacrylamide gel electrophoresis
PPI	Protein-protein interaction
RAN	Ras-related nuclear protein
SDS	Sodium dodecylsulfate

SEC	Size exclusion chromatography
SPR	Surface Plasmon resonance
Sulfo-NHS	N-hydroxysulfosuccinimide
TCEP	Tris(2-carboxyethyl)phosphine
TEMED	Tetramethylethylenediamine
UNC-76	Uncoordinated-76

Contents

1. Introduction

1.1. Histone Deacetylase 6 (HDAC6)

1.1.1. Classification of HDACs

There are 18 identified members of a mammalian histone deacetylase (HDAC) family based on sequence homology.(1) The main function of these enzymes is deac(et)ylation of modified lysine side chains. The deacetylation influences many cellular processes including transcription, cell signalling, cell cycle kinetics, cell motility, cellular transport and cell death.(2)

HDACs are classified into four classes.(1) Class I consists of HDAC1, HDAC2, HDAC3 and HDAC8, which are located mainly in the nucleus. They are predominantly responsible for histone deacetylation and repression of gene transcription. Class II comprises two subclasses, Class IIa (HDAC4, HDAC5, HDAC7 and HDAC9) and Class IIb (HDAC6 and HDAC10), which shuttle in between the nucleus and the cytosol but HDAC6 is mainly located to the cytosol. Class III consists of sirtuins, non-classical HDACs with a distinct NAD^+ dependent hydrolytic mechanism.(3) HDAC11 is the only member of Class IV.(1)

1.1.2. Deacetylase Activity of HDACs

Acetylation is a major posttranslational modification in the cell. It modifies the α-amino group of polypeptide N-termini or the ε-amino group of lysine side chain (Figure 1). The acetyl group originate from acetyl-coenzyme A and it is transferred to the amino group by N-terminal acetyltransferases (NATs) and lysine acetyltransferases (KATs).(4) Whereas the N-terminal acetylation is considered irreversible, the lysine modification is reversible, and the deacetylation is catalysed by HDACs.(5)

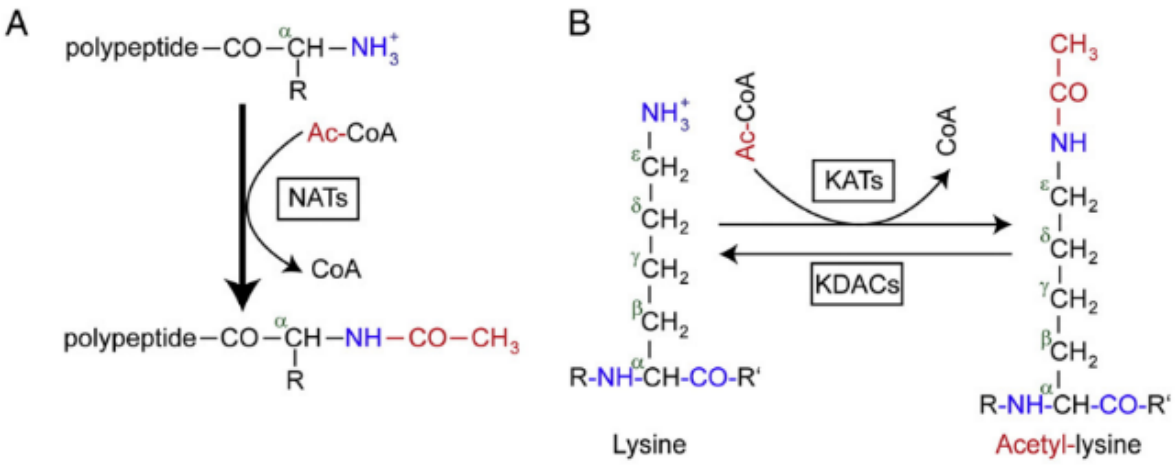

*Figure 1 - Acetylation/deacetylation of N-terminal amino group (**A**) and lysine side chain (**B**) (Taken from Drazic et al., 2016)*

The lysine acetylation occurs not only at histones but also at many other proteins. For this reason, histone deacetylases (HDACs) are also known as lysine deacetylases (KDACs). The acetylation of histones (along with other posttranslational modifications) induces heterochromatin-euchromatin transition.(6)

HDAC6 is the major tubulin deacetylase of α-tubulin. α and β-tubulin heterodimers are the building units of microtubules. Microtubules are directional cytoskeletal filaments involved in cell motility and intracellular transport. Lysine-40 of α-tubulin is the target for HDAC6 and this modification plays a role in the microtubule dynamics.(7) HDAC6 inhibition leads to α-tubulin hyperacetylation. On the other hand, HDAC6 overexpression leads to reduced microtubule acetylation and higher cell motility.(8)

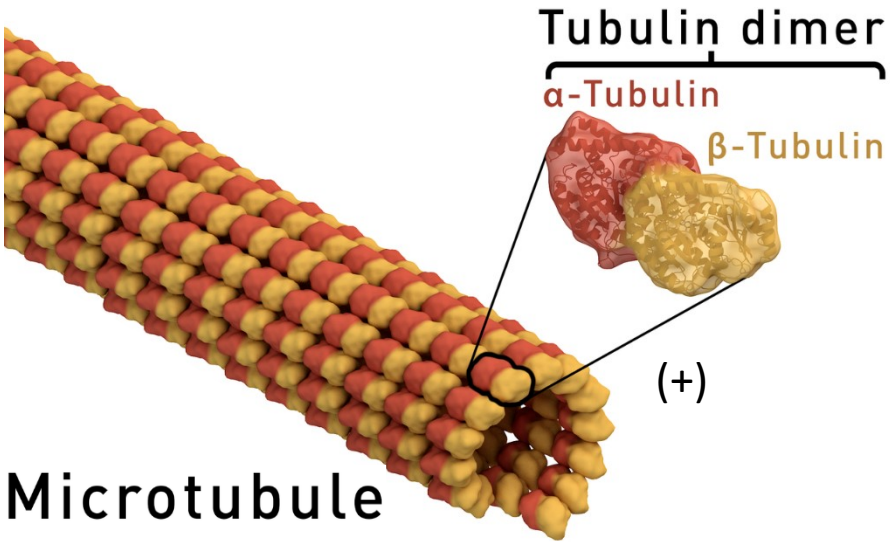

Figure 2 – Schematic picture of a microtubule structure

(Taken from https://commons.wikimedia.org/w/index.php?curid=41014850, by Thomas Splettstoesser (www.scistyle.com), April 12, 2019)

A microtubule is a cytoskeletal filament composed of α-tubulin (orange) and β-tubulin (yellow). It has a plus and a minus end.

1.1.3. Structure of HDAC6

HDAC6 is a multifunctional protein of 1215 amino acid residues that is composed of several domains and sequence motifs (Figure 3). The enzyme is composed of 1215 amino acid residues. The N-terminal domain is probably unstructured (Figure 4) and it is responsible for microtubule binding (unpublished data). There are two tandem deacetylase domains, DD1 and DD2, with 48% sequence identity.(9) A linker in between these two domains contains a dynein binding motif. The SE14 domain contains a cytoplasmic anchoring sequence and at the C-terminus there is a binding of ubiquitin zinc finger domain (BUZ).(7)

HDAC6 is predominantly localized to the cytoplasm as it contains a nuclear exclusion signal (LVVGLQGLDL) in the N-terminal domain and a cytoplasm anchoring SE14 repeat motif

(SExAxGGATLxQTx).(10, 11) When the cell proliferation is blocked, a fraction of HDAC6 shuttles to the nucleus.(11)

Figure 3 – Schematic representation of HDAC6 domains

N – N-terminal domain, DD1 – deacetylase domain 1, L – linker with dynein binding motif, DD2 – deacetylase domain 2, SE14 – SE14 domain, BUZ –C-terminal binding of ubiquitin zinc-finger domain

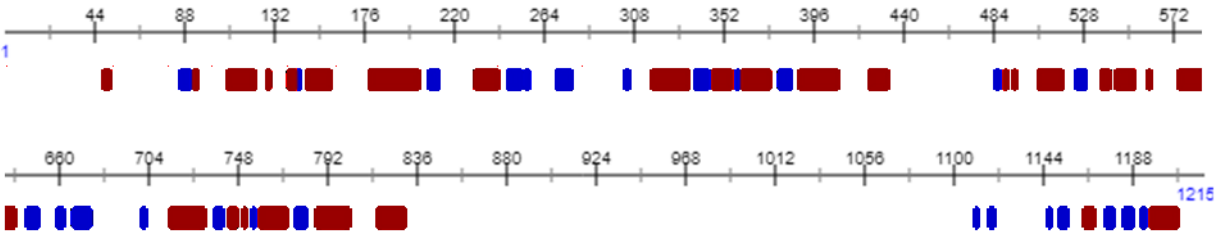

Figure 4 - Prediction of HDAC6 secondary structure

α-helices in red, β-sheets in blue under corresponding numbers of amino acids

Structures of the human DD2 and BUZ domains have been solved by X-ray crystallography (Figure 5).(12, 13) Also, there is a 3D structure of *D. rerio* HDAC6 DD1 and DD2 domains (14). A structure of the both catalytic domains of the human homolog together has not been solved yet. The reason is probably a ten amino acid longer linker between the catalytic domains that is negatively charged due to the presence of several glutamate residues. The structure of human and *D. rerio* DD2 are very similar as shown in a structural alignment in Figure 5. The active site contains a Zn^{2+} ion and it is involved in the catalytic process. There are two K^{+} ions coordinated in the structure of DD2 that probably contribute to stability of the domain.

The secondary structure prediction (Figure 4) shows that the N-terminal domain (amino acids 1-84), the linker in between DD1 and DD2 (amino acids 440-480) as well as the SE14 domain (835-1109) are most likely unstructured.(15) That is most likely the reason why the structure of the full length protein is not known.

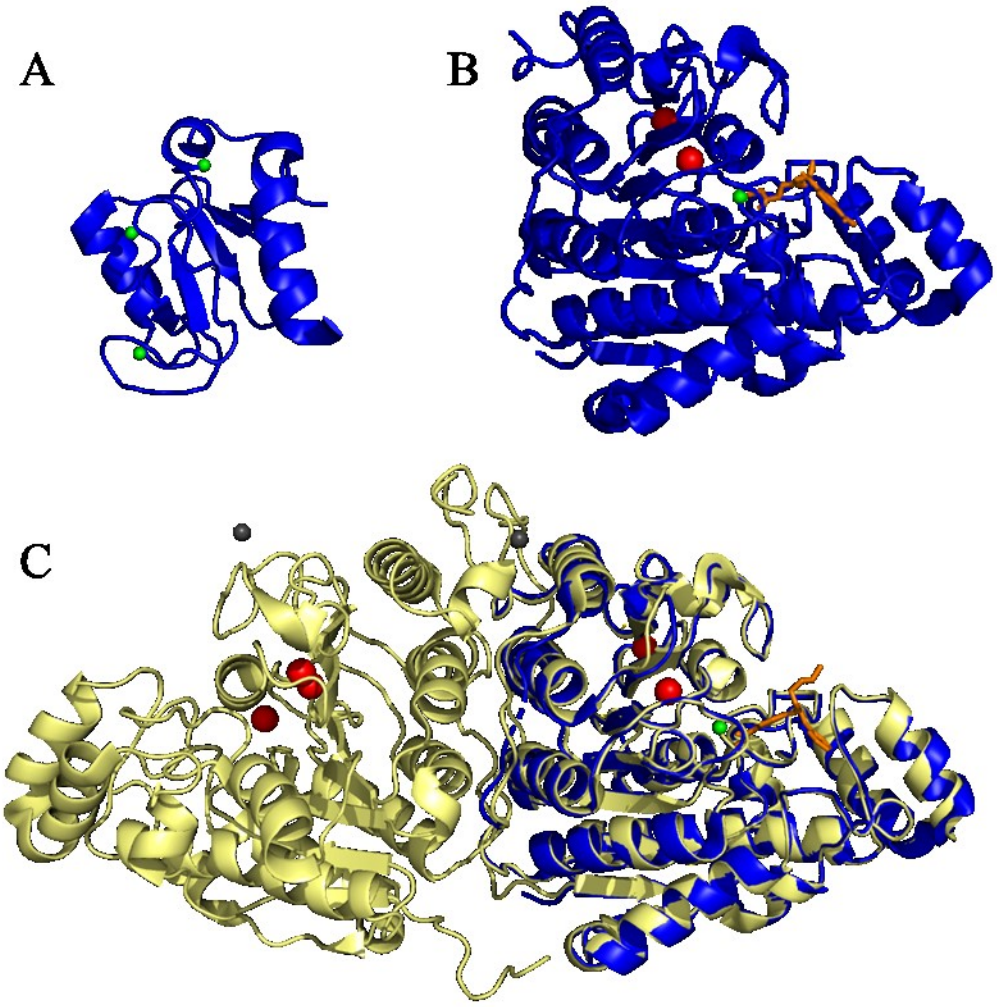

*Figure 5 – A structure BUZ (**A**), and DD2 (**B**)domains of human HDAC6. Superposition of human DD2 and DD1-DD2 from Danio rerio HDAC6 (**C**)*

BUZ and DD2 domains of hHDAC6 are in blue, DD1 DD2of drHDAC6 is in yellow, Zn^{2+}, K^{+} and Cl^{-} ions are shown as green, red and grey spheres, respectively, an HDAC6 inhibitor is in stick represenatation (orange). PDB codes: 5kh3, 5edu, 5g0j

1.1.4. Role of HDAC6 in Cancer

HDAC6 plays an important role in many microtubule-dependent processes, since HDAC6 is an α-tubulin deacetylase.(1) Overexpression of HDAC6 is associated with several cancers – breast cancer (16), glioblastoma (17), ARID1A mutated ovarian cancer (18) and multiple myeloma (19). Additionally, HDAC6 is necessary in tumour cells to be resistant to anoikis (a programmed cell death when the cell is detached from their peripheral matrix). Therefore, HDAC6 facilitates tumour cell invasion and metastasis.(20) As HDAC6 knock-out mice are viable, it is a suitable target for cancer therapy.(7)

Misfolded proteins are being accumulated in cancer cells.(21) They must be degraded through either the ubiquitin-proteasome system or the aggresome-autophagy pathway.(21, 22) HDAC6 binds ubiquitinylated misfolded proteins by the BUZ domain and mediates their transport via dynein molecular motors to microtubule organising centre where the aggresome is formed.(22) Proteasome inhibitors suppress disposal of misfolded proteins by the ubiquitin-proteasome system. In combination with HDAC6 inhibitors they could enhance the effect of the proteasome inhibitors by increasing the toxicity of accumulated misfolded proteins in the cells as they inhibit both degradation pathways.(23)

A mutation in the *ARID1A* gene in an ovarian cancer upregulates HDAC6 expression. HDAC6 deacetylates p53 which reduces its pro-apoptotic regulating function. Therefore, the ARID1A mutation leads to inactivation of p53 pro-apoptotic function. Mice treated with the HDAC6 inhibitor ACY1215 showed much higher overall survival compared to untreated mice.(18)

HDAC6 is also overexpressed in human glioblastoma cells. This type of tumour is highly resistant to chemotherapy and radiotherapy. HDAC6 inhibition increases the sensitivity of the glioma cells to the treatment.(17)

HDAC6 is an estrogen-regulated gene overexpressed in an estrogen receptor α positive breast cancer. The overexpression causes higher cell motility and migration ability of the cancer cells. Antiestrogen treatment downregulates HDAC6 expression and together with HDAC6 inhibitor tubacin treatment reduces cell motility. These facts suggest a survival benefit for the patients to be treated with antiestrogen agents and HDAC6 inhibitors.(16, 24)

Non-selective HDAC inhibitors are studied as therapeutics in multiple myeloma and, also, in a combination with proteasome inhibitor bortezomib they block both the proteasome and aggresome misfolded protein degradation pathway.(19) Based on this information, ACY-1215 was tested as the toxicity of HDAC6 selective inhibitors is much lower than non-selective HDAC inhibitors because HDAC6 knock-out mice are viable unlike HDAC1, 2 and 3 knocked-out mice.(7, 19) This combination shows an synergic effect in the tumour cells treatment.(19)

1.1.5. Role of HDAC6 in Neurodegenerative Disorders and Its Connection with Intracellular Transport

Accumulation of misfolded proteins is harmful to the cell. Therefore, it is no coincidence that the accumulation of protein aggregates is a common feature of many neurodegenerative disorders. The accumulation overwhelms the proteasome degradation pathway resulting in even higher accumulation of highly ubiquitinylated misfolded proteins observed in afflicted neurons of Alzheimer's and Parkinson's diseases.(25)

HDAC6 is involved in mechanisms of protein aggregates disposal in the cell. HDAC6 can increase the cell viability by binding polyubiquitinylated misfolded proteins via its C-terminal zinc-finger domain (BUZ), which leads to active transport of these proteins dispersed in the cytoplasm and contributes to the formation of the aggresome that can be latter cleared by autophagy.(25-29) More accurately, polyubiquitinylated misfolded protein aggregates are transported by the dynein motor protein complex to form the aggresome. HDAC6 439-503 amino acids are responsible for interaction with the dynein motor complex. The dynein motor proteins bind HDAC6 associated with the polyubiquitinylated misfolded proteins and transport them to the aggresome located in proximity of the microtubule-organising centre. HDAC6, thanks to its several domains, has the capacity to bind dynein motor and polyubiquitinylated misfolded proteins at the same time which would explains why it is indispensable for the aggresome formation.(27)

HDAC6 is phosphorylated at Ser458 by CK2 kinase which results in upregulation of its deacetylase activity. Presence of CK2 kinase increases binding between HDAC6 and the dynein motor complex even if the kinase is expressed as a non-active mutant.(30) Moreover, HDAC6 phosphorylation performed by HEF1, AurA and GRK2 kinases enhances HDAC6 tubulin deacetylation activity. (31, 32)

Another feature linked to neurodegenerative disorders is decreased mitochondrial transport connected with a deacetylase and an ubiquitin binding function of HDAC6. (33) HDAC6 plays a role in regulation of microtubule-dependent intracellular trafficking via the Akt-GSK3-β signalling pathway.(34) HDAC6 is one of GSK-β's targets,(33) tubulin is a major substrate for HDAC6 and inhibition of HDAC6 strongly increases the acetylation of tubulin in vivo and in vitro.(35, 36) GSK3-β inhibition increases the microtubule acetylation and improves the mitochondrial transport.(37) Moreover, a tubacin treatment (HDAC6 inhibition) of hippocampal neurons also enhances the mitochondrial movement. Both treatments result in highly acetylated tubulin and enhances binding of kinesin-1 as well as dynein molecular motors to microtubules leading to promotion of the cargo transport along microtubules. (34, 38) In case of HDAC6 inhibitors, both the velocity and the number of moving mitochondria is increased. Unfortunately, it is unclear how the tubulin acetylation enhances the trafficking of cargos along microtubules.(38-40)

HDAC6 can be found in a single complex with GSK3β and kinesin. HDAC6 inhibition increases not only the affinity of kinesin to microtubules due to higher acetylation but also the kinesin velocity. This phenomenon can have many explanations. One of them is that inhibited HDAC6 does not bind to microtubules so that there are less obstacles on the microtubule the kinesin must step to a side from.(41) Other one is that the free inhibited HDAC6 participates in the activation. Also, the molecules of kinesin can move one cargo together with higher velocity (42) and they can be activated/linked by those inhibited HDAC6 molecules. In the experimental part of this thesis the interaction between kinesin (KIF5B) was analyzed to confirm or refute the hypothesis HDAC6/kinesin interaction.

1.2. Kinesin-1

The cell needs various molecules and organelles to be transported throughout the cytoplasm. The molecular machinery for intracellular transport is well conserved for all cell types even though the transport is crucial especially for neurons with their long axons and dendrites. This transport is provided by microtubule associated motor proteins kinesins and dyneins. The motor proteins walk along the microtubules with determined directionality. Dynein steers towards the minus end of the microtubule, while kinesins move towards the plus end of the microtubule.(43)

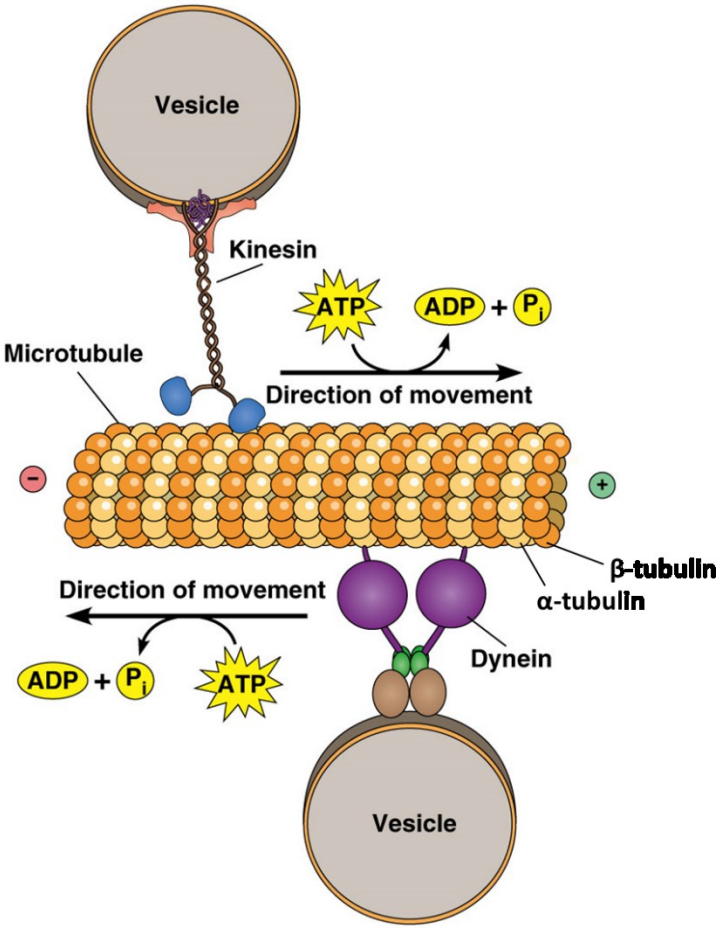

Figure 6 - ATP-dependent molecular motors walk along a microtubule

(Taken from http://www.mun.ca/biology/desmid/brian/BIOL2060/BIOL2060-16/CB16.html, April 2 2019)

Kinesin-1, also known as a conventional kinesin, is a kinesin family composed of three members KIF5A, KIF5B and KIF5C. KIF5B, which is the subject of the thesis, is the best studied family member. KIF5B and KIF5A have the 72 % sequence identity and KIF5B and KIF5C have the 76 % sequence identity.(9)

1.2.1. Kinesin-1 Structure and Autoinhibition

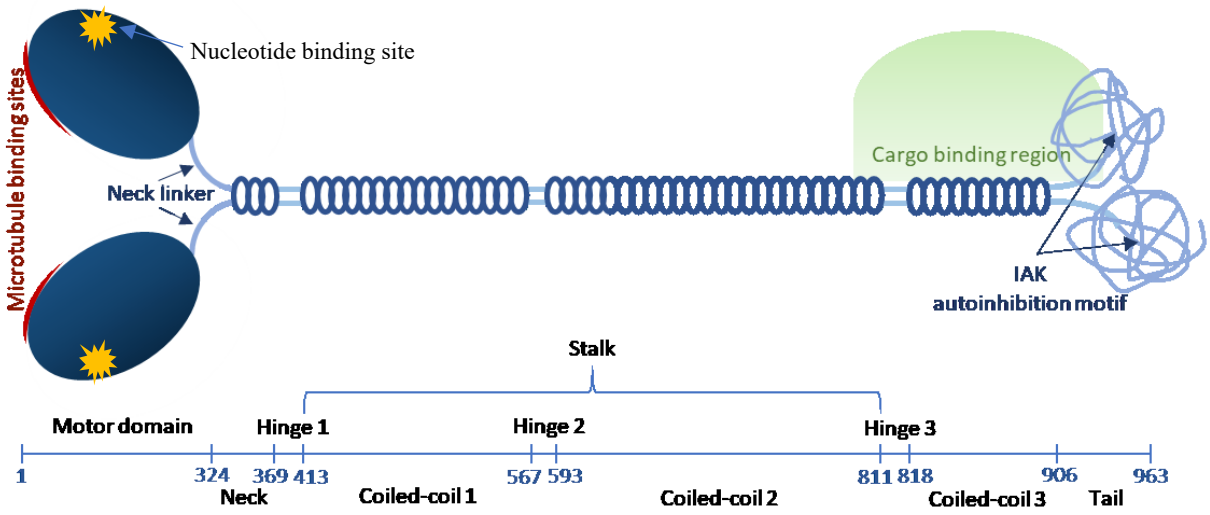

Figure 7 – Schematic representation of kinesin homodimer

In the cell, kinesin (below meaning kinesin-1 if not specified) can be a homodimer composed of two heavy chains or a heterotetramer composed of two heavy and two light chains. The heavy chain of kinesin consists of a motor domain at the N-terminus also known as the head (Figure 7). This domain interacts with microtubules and has an ATPase activity (Figure 11). There is a linker between the head and a coiled-coil domain called the neck linker. The coiled-coil domain, stalk, provides the tight interaction between two heavy chains creating the homodimer. There is a tail domain at the C-terminus which is responsible for autoinhibition of kinesin via interaction with the motor domains. This fact means that the stalk's crucial characteristic is its flexibility so the tail can bend to the head. The flexibility is provided via three hinges, unstructured parts that connect the coiled-coils regions (Figure 8).(15)

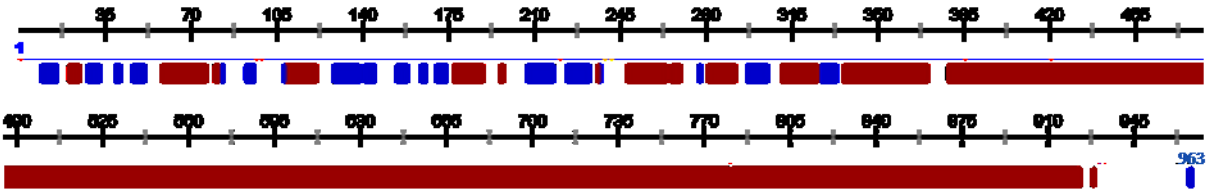

Figure 8 – Prediction of kinesin-1 secondary structure

α-helix in red, β-sheet in blue under corresponding numbers of amino acids

Kinesin movement must me tightly regulated to prevent futile ATP hydrolysis and to allow fast spatio-temporal control of kinesin trafficking. If kinesin does not have a binding partner, it is folded in an autoinhibited state where the C-terminal domain is bound in between the N-terminal motor domains through an IAK motif and blocks its ATPase activity (44) and high affinity interactions with

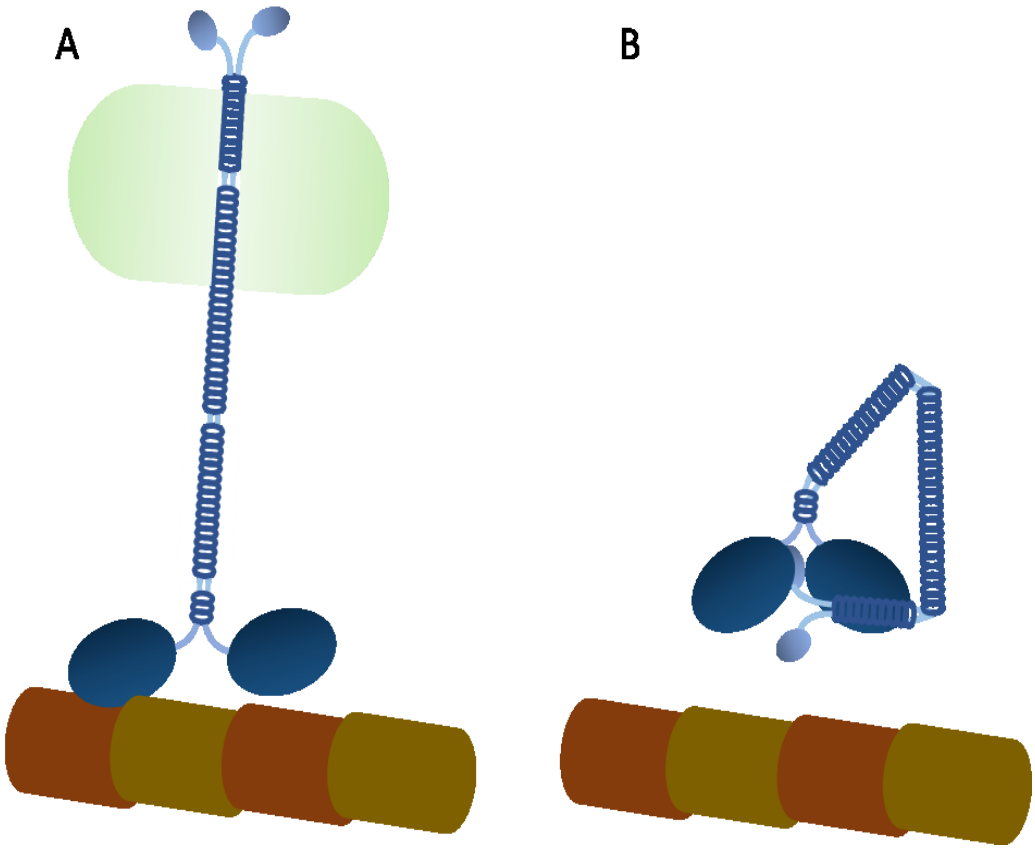

Figure 9 - Autoinhibition of kinesin via head-to-tail interactions

A Kinesin activated by interaction with cargo (light green) walking along microtubule, B Autoinhibited kinesin detached fram the microtubule

microtubules (Figure 9). When the kinesin is autoinhibited, ADP is bound very tightly to the motor domain .(45) Only one of the tail domains of the homodimer binds to the motor domains and inhibits the ADP release and microtubule interaction.(44) The interacting part of the tail has an extended linear conformation even though it is probably unstructured in its free state (Figure 8). The conformational change affects the distance in between the motor domains, which is restricted while autoinhibited.(44) When the light chains are present, they add another regulatory factor as they push the two motor domains apart.(45) When the autoinhibition is turned off by an interaction with a cargo, the motor domains are connected via the flexible stalk segment so that they can make steps and their affinity for ATP/ADP and microtubules changes in cycles of the motor domain steps (described in Chapter 1.2.2.).

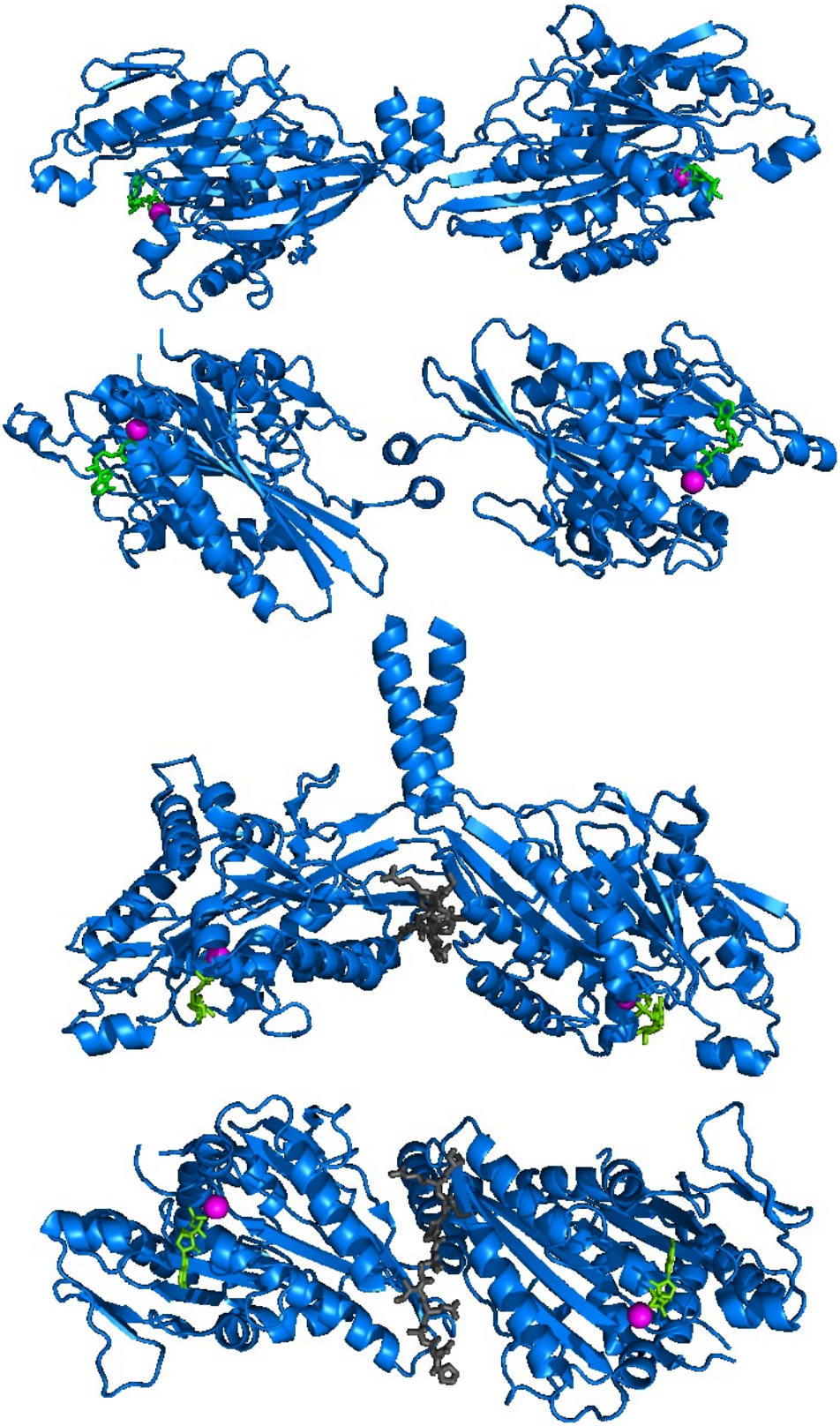

Figure 10 – Structures of kinesin motor domains connected via part of the coiled-coil domain

Kinesin motor domains in blue, Mg^{2+} ions in magenta, ADP in green and inhibitory part of tail domain in gray. ***A*** *A side-view of not autoinhibited motor domains,* ***B*** *A bottom-view of not autoinhibited motor domains,* ***C*** *A side-view of autoinhibited motor domains,* ***D*** *A side view of autoinhibited motor domains. PDB codes: 2y65, 2yw5*

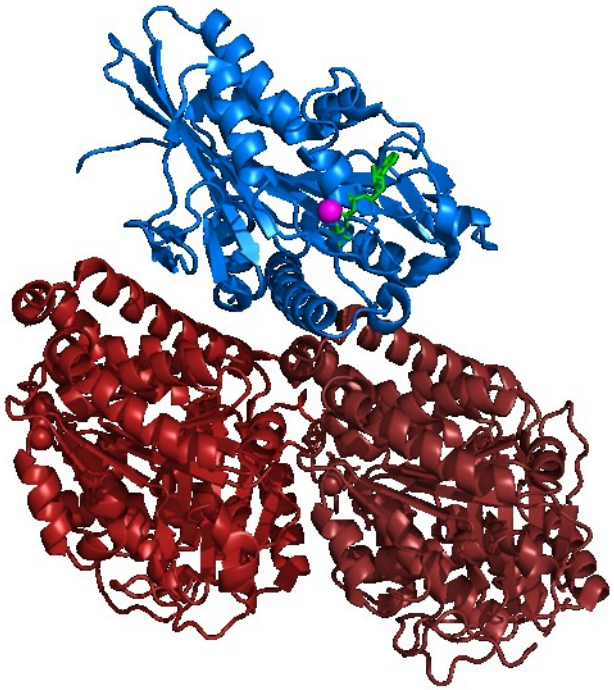

Figure 11 - Structure of kinesin motor domain in complex with a tubulin dimer

Kinesin motor domain is in blue with ATP-PNP in green and Mg^{2+} ion in magenta color. Tubulin dimer is in dark red. PDB code: 4hna

1.2.2. Chemomechanical Cycle of Kinesin-1 Walking

The molecular mechanism of kinesin processivity is considered gated, meaning that transitions occurring in one head are controlled (gated) by activity of the other head.(46, 47) During one step, for a half of the time both heads are bound to the microtubule (2HB state), and for the other half only one head is bound to the microtubule (1HB state, Figure 12). When the head is bound to the microtubule, it can bind ADP, ADP + Pi, ATP or no co-factor. When the head is not bound to the microtubule, it binds ADP. The affinity of the head/co-factor binding depends on the interaction between the head and the microtubule. (48)

As of the starting point is the 2HB, the hinder head is bound tightly to the microtubule and it also binds ADP and inorganic phosphate. The leading head binds ADP so that its interaction with the microtubule is weak (Figure 12, State 1). Then, the ADP from the leading head is released resulting in tight binding to the microtubule (State 2) because the ADP affinity is reduced by the tension of the binding to the microtubule.(48) The inorganic phosphate is released from the hinder head and its interaction with the microtubule weakens (State 3).(49) The transition between state 2 and 3 is rate-limiting transition in the 2HB part of the cycle. The leading head binds ATP (State 4) which results in rapid detaching of the hinder head from the microtubule (State 5). Now, we are in the stable 1HB state. When the ATP at the microtubule-bound head is hydrolysed (State 6),(50) the 1HB state is vulnerable meaning that the

kinesin can detach form the microtubule at this point (<1 % for kinesin-1). If the detachment does not happen, the tethered head finds the next binding spot on the microtubule resulting it the 2HB again.(51)

During 2HB phase, the ATP binding occurs and ATP hydrolysis induces the transition from 1HB to 2HB.(50) In more detail, the binding of ATP to the front head in state 4 triggers a power stroke induces the conformational change resulting in fast detachment of the hinder head, meaning, ATP binding induces a partial rotation of the catalytic motif of the head in a perpendicular direction to the microtubule axis opening a gap for the neck linker. (52-54) The linker consequently changes its conformation resulting in the kinesin gated movement as it is the part of the molecule connecting the microtubule attached head with the stalk and the other head.(55)

Processivity is defined as a number of steps a molecular motor takes before it detaches from the microtubule and it is among other things dependent on the length of their neck linker. The neck linker of kinesin-1 is 14 residues long. (47) Longer neck linkers are associated with lower processivity.(56) When the neck linker of other kinesins were shortened to 14 residues, their processivity was identical to kinesin-1.(47) An explanation for existence of longer neck linkers is easier adaptation to sidestepping around obstacles. (56)

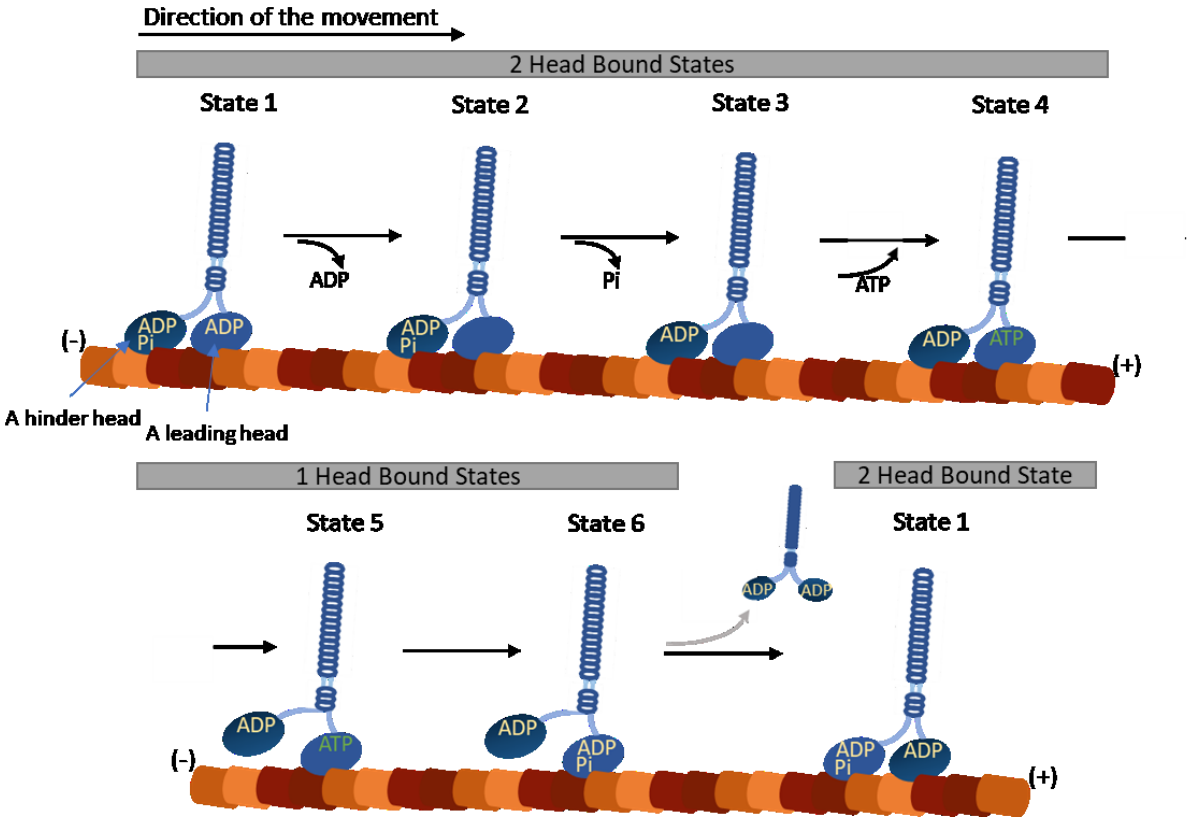

Figure 12 - A process of one kinesin step on a microtubule

1.2.3. Kinesin-1 Activation and Functions

As mentioned above, free kinesin in autoinhibited and it needs to be activated to walk and transport its cargos. In general, kinesins are activated by interaction with adaptor or scaffold proteins which provide the linkage to their cargos, even though there are some examples of direct interactions with transmembrane proteins of transported vesicles.(57) All kinesin-1 binding/activating proteins typically have additional physiological functions. Numerous transmembrane and peripheral membrane proteins interact with kinesin activators and many proteins from signalling pathways are regulators of interactions between cargos and kinesins.(58)

Functionally, kinesin is associated with membrane bound organelles (the endoplasmic reticulum, the Golgi complex, mitochondria and lysosomes).(59) The interaction is pH and salt concentration dependent and trypsin treatment of the organelles blocks their interaction with kinesin.(60)

Kinectin was the first kinesin binding protein discovered. It is a membrane-associated protein found on the surface of the endoplasmic reticulum and it is also a microtubule-associated proteins.(61) This protein interacts with the C-terminal coiled-coil 3 of kinesin and mediates lysosome transport.(62)

JIP1 (c-Jun N-terminal kinase interacting protein) binds to a kinesin light chain, but it does not activate the kinesin heterotetramer. As the FEZ1 protein binds to the autoinhibitory tail of the kinesin heavy chain, in cooperation with JIP1, FEZ1 activates the kinesin heterotetramer.(63) Moreover, overexpression of *Drosophila* JIP1 causes accumulation of synaptic proteins in axons and larval-pupal lethality similarly to phenotypes with kinesin heavy and light chain mutations. The pathology may be caused by competition between JIP1 and other kinesin binding proteins that attach kinesin to other cargos.(64)

UNC-76 is a Drosophila homolog of the mammalian FEZ1 protein and a specific binding partner of the tail domain of the kinesin heavy chain. UNC-76 is a cytosolic protein which is important for nervous system function. Mutations of UNC-76 has a neuromuscular effect similar to kinesin-1 mutants.(65) Overexpression of FEZ1 leads to enhanced neurite outgrowth.(58) There are numerous known binding partners of this protein complex illustrating the variability of kinesin cargo transport. UNC-76/FEZ1 interaction with kinesin-1 regulates its activity in cooperation with its binding partners. Some of them enhance FEZ1 dependent increase of neurite outgrowth (protein kinase C, ubiquitin ligase E4B, mitochondria-associated protein disrupted in schizophrenia 1, Prader-Willi syndrome protein necdin) while agnoprotein inhibits it.(66-70)

The RAN-binding protein 2 interacts with approximately 100-amino acid segment of kinesin at C-terminal coiled-coil 3 and tail domain (KIF5B and KIF5C) through its kinesin-binding domain. It works as an allosteric activator of kinesin. Kinetics of KIF5B and RAN-binding protein 2 is biphasic and highly cooperative. The kinesin-binding domain of the RAN-binding protein 2 is responsible for their

interactions but the RAN GTPase-binding domains, which are on both sides of the kinesin-binding domain, are responsible for the activation. There are four binding sites on kinesin in the interaction kinetics of this complex and the maximum activity is observed only when all four of them are occupied.(71) From the biological point of view, mutations in the RAN-binding protein 2 are linked to various infections leading selectively to necrosis of neurons in the central nervous system.(72) However, selective inhibition of the interaction between the kinesin-binding domain of the RAN-binding protein 2 and kinesin causes peri-nuclear localization of mitochondria, deficits in mitochondrial membrane potential and cell shrinkage.(73)

Other macromolecules such as RNAs, are also transported by molecular motors. A directed kinesin transport of mRNAs is crucial for nervous system development and establishment of the dorsal/ventral and anterior/posterior axes of differentiation during embryogenesis.(74) mRNA molecules are transported in large complexes with the fragile X mental retardation protein and many other proteins.(75) It has been shown, that only the heavy chain of kinesin is required for transport of the fragile X mental retardation protein since light chain disruption has no effect on its function in *Drosophila* cells.(76, 77) It is worth mentioning that kinesin heavy chain-mRNA interference results in depletion of not only the heavy chain but also the light chain. An explanation for this fact is co-translational association of light chains with heavy chains as the kinesin light chain is immediately degraded when it is translated alone. These facts point out that some kinesin molecules in the cell are in the conformation of homodimer without the light chain and that the stalk interaction with the activation proteins are as important as interactions with the light chains. (76)

Overall, the activation of kinesin molecular motors is complex and requires a large binding interface (e. g. a 100-amino acid segment) as it results in a huge conformational change of the kinesin heavy chain. Typically, more than one domain (RAN-binding protein 2) or protein (JIP1/FEZ1) are necessary for the activation. (63, 71) Additionally, interaction of GRIP1 with kinesin is necessary for transport of kinesin-1 cargos within dendrites. GRIP1 is a scaffold protein binding the mouse kinesin heavy chain. Loss of this protein causes defected dendrite formation, embryonic lethality and epidermolysis bullosa which illustrates the importance of kinesin proper transport in development and differentiation.(78, 79)

1.3. Protein-Protein Interactions and Techniques to Analyze Them

More than 80 % of proteins operate in complexes with other proteins. (80) A huge variety of biological processes such as cell-cell interactions and various signal transduction pathways managing cell metabolism and development are based on protein-protein interactions (PPIs).(81) Functionality of unidentified proteins may be predicted based on their known interacting partners.(82)

PPIs can be described from different angles and one of the most important to analyze is the stability of PPIs.(82, 83) PPIs are evolved for their biologically efficient functionality. In some cases, the low affinity is necessary for the function e. g. cell shape formation and migration,(84) although the high affinity is indispensable in others, e. g. interaction between antigen and antibody.(85)

PPIs can be obligate or non-obligate. In cases of obligate PPIs, the proteins exist only in the complexes, as they are usually connected co-translationally. The non-obligate PPIs are much more common and can be found e. g. between an antibody and an antigen or a receptor and its ligand.(85) The non-obligate interactions can be stable or transient. Generally, PPIs in signalling pathways are mostly transient while multifunctional complexes are more stable.(82)

Noncovalent interactions among sidechains form the basis for PPIs as well as protein folding.(82) The hydrophobic collapse driven by increase of water entropy is the main driving force for protein folding so that the surface of proteins is polar. Interfaces of PPIs are quite polar as well so that formation of a protein-protein complex results in burying polar and charged residues.(86) However, obligate complexes are the only group of protein complexes that has hydrophobic interfaces but even in this case the hydrophobic residues are scattered in small patches and do not cover large parts of the surface.(83) Also, interfaces in obligate complexes are generally larger. Non-obligate complexes have more polar interface as necessary for independent existence and solubility of the free proteins.

An average PPI interface (about 800 $Å^2$ per monomer) was found to have about ten intermolecular hydrogen bonds and two salt bridges. The distribution of residues responsible for these interactions can explain high specificity of PPIs.(87) As a matter of fact, electrostatic interactions increase the time which two proteins stay close to each other allowing them to rotate into a suitable orientation for binding. The desolvation effect is then partially compensated by the formation hydrogen bonds and salt bridges as they are positioned to interact favourably with each other.(86) Actually, most of the PPIs are highly specific even though they have multiple binding partners, the binding interfaces are different or slightly overlapped. Paralogues have usually different specificities within a generic class of binding partners.(85)

The characteristics of PPIs of intrinsically disordered proteins (IDP) or regions of proteins are a bit different and much less investigated. These IDPs function by molecular recognition so that they are parts of protein complexes.(88) Our current understanding is that IDPs are structurally disordered in isolation, they are structured in a complex with their binding partner. Often, parts of the proteins or the protein complexes cannot be described in a single conformation even though they contribute to binding and function of the complex. They can occupy several diverse conformations or exist is continuous distribution of conformations. These conformations can even have different functions.(88)

Affinity of interaction between proteins can be characterized by a dissociation constant K_D as interaction between any other molecules. The simple interaction between two molecules can be described by a following equation:

$$A + B \rightleftharpoons AB$$

Then the K_D is described as equilibrium concentrations of A, B and the complex AB.

$$K_D = \frac{[AB]}{[A]\,[B]}$$

In many cases of PPIs, the interaction in more complicated so that this model does not describe it. There are many other more complicated equations describing these complicated interactions. One of them, which is commonly used, is the Hill model. It includes a parameter of cooperative binding of several molecules of ligand.

$$P + nL \rightleftharpoons PLn$$

$$\theta = \frac{[L]^n}{K_D + [L]^n}$$

θ is a fraction of a protein bound to a ligand L, [L] is a concentration of an unbound ligand, K_D is an apparent dissociation constant derived from the law of mass action and n is a Hill coefficient describing cooperativity of a ligand binding. (89)

To determine EC50 (half maximal effective concentration, concentration that provokes a response half way between the bound and unbound plateau) of interacting partners with log(dose) response curve with a symmetrical sigmoidal shape – Variable slope can be used. It is a four-parameter dose-response curve.

$$Y = Unbound + \frac{X^{Hillslope} * (Bound - Unbound)}{(X^{Hillslope} + EC50^{Hillslope})}$$

Y is value in response units that the y axis is in, unbound/bound is a response value of the unbound/bound plateau, $X^{Hillslope}$ is concentration of a ligand in dilution series exponentiated to Hillslope value.

Many techniques have been developed for measurement of these binding constants using various ways of detection. In this thesis, microscale thermophoresis and surface plasmon resonance have been used and the principles are described below. Also, the interaction can be studied from the structural point of view. For this purpose, mass spectrometry detection was used to analyze hydrogen/deuterium exchange and chemical cross-linking. Principles of these methods are described below.

1.3.1. Microscale Thermophoresis

Microscale Thermophoresis (MST) is a technique for biomolecular interaction quantification. It can be used to analyze a large variety of interactions between proteins, oligonucleotides, proteins and DNA, proteins and liposomes, proteins and small molecule ligands.(90) The principle of this method is observation of thermophoresis (a directed movement of particles in a temperature gradient) in a few microliter volume, which is highly sensitive to changes in molecular hydration shell. The hydration shell is changed by binding of other molecule or any change of its conformation. Changes of these properties can be caused by any interactions between fluorescent molecules and their ligands or binding partners.

The temperature gradient is created by an infrared laser and the movement is detected via a change in a fluorescence signal. Fluorescence can be intrinsic (tryptophan) in a case of a protein and another non-fluorescent molecule or extrinsic from fusion fluorescence proteins or other fluorescence labelling. A big advantage of MST is that it does not require any immobilization. (90)

The experiment is performed in small glass capillaries containing the solution of analyzed molecules. The infrared laser produces a microscopic 2-6 °C temperature gradient with a diameter of 50 μm. The fluorophores are excited, and the ensuing depletion or accumulation of the molecules is detected for about 30 seconds. To derivate the binding constant, a dilution series of non-fluorescent molecules mixed with the same concentration of fluorescent-labelled molecules are measured. For analyses, the change in thermophoresis is usually evaluated as a normalized fluorescence signal defined as a quotient of a fluorescence signal of a heated sample and a non-heated sample. Also, in the first seconds after infra-red laser activation, a T-jump is observed. It is a fast decrease of the fluorescence quantum yield and it corresponds to a rapid change in fluorophore surroundings by ligand binding and can be used to determine the binding affinity as well. On the other hand, thermophoresis depends on the overall properties of the particle and the differences are detected in a scale from a few seconds to a minute. (90)

1.3.2. Surface Plasmon Resonance

The phenomenon of surface plasmon resonance (SPR) is used for characterization molecular interactions. SPR occurs on the surface of some metals (Au, Ag, Cu, Ti) when lightened by a light ray under a certain angle. Surface plasmons induced by the light ray are electromagnetic waves parallel to the surface of the thin metal layer (tens of nm). They originate from oscillations of electron density of the metal. The intensity of the reflected light is reduced due to genesis of the plasmons. They depend very sensitively on thickness of a mass layer (resp. on the refractive index on the layer) on the metal. Interactions of molecules in the solution with molecules immobilized on the surface of the metal increase the mass layer and change the detected refractive index.(91)

There are several options of sensor chips with different principles of immobilization. The sensor chips can have different binding capacities depending on the length of the functionalized matrix on the metal surface. Amine coupling sensor chips are the most common type of chips. The immobilized proteins do not need to have tags or modifications because they are bound to the surface matrix via their N-terminal or lysine side chain amine groups (the same principle of binding like chemical cross-linking, Figure 13). Biotinylated molecules can be specifically immobilized on the neutravidin modified surface. Immobilization of polyhistidine tagged proteins is also possible. The chips matrix is modified by the tris-NTA. The immobilization can be a problem because of special conditions required for amine coupling, which may be harmful for the ligand, or the non-specific interactions of analytes with the modified surface of the sensor chip.(91)

The main advantage of SPR as a method for studying PPIs is the possibility to measure the affinity and kinetics of association and dissociation in real time. Also, the experiments can be done in a label-free environment using relatively small amounts of proteins and this method can detect binding of highly dynamic complexes. In SPR terminology, the protein immobilized on the surface of the sensor chip is called a ligand and the protein interacting with this immobilized ligand is called an analyte. When the ligand is immobilized on the sensor chip, the analyte is flushed in and signal value changes in response to the mass bound on the chip. At the same time, the analyte is flushed in a control channel with no ligand on the sensor chip as the reference of change in refractive index from the present mass. The value of this control is than subtracted from the signal in the measuring channel. The flush-in phase is the association phase and the association curve can be used to calculate the rate of association (k_a). When the steady state is reached, the association and dissociation events are equal, the binding affinity (K_D) can be calculated form this part of the curve. The flow of the analyte solution is replaced by a buffer and the dissociation of the analyte from the ligand induces decrease in the refractive index. This part of the curve is used to calculate the rate of dissociation (k_d). The experiment is followed by a regeneration step to remove the remaining analyte molecules. It can be performed by different types of solutions (low pH, high ionic strength) depending on a type of a sensor chip, a ligand and an analyte.(91)

1.3.3. Chemical Cross-Linking Connected with Mass Spectrometry

Studying of a protein three-dimensional structure and identification of its interaction sites with a binding partner is in a tight relation with studying the protein functions. Alternatives to high resolution methods for 3D structure determination such as NMR spectroscopy and X-ray crystallography are low resolution methods including cross-linking and hydrogen/deuterium exchange using mass spectrometry analysis which enable an insight into the 3D structure of proteins or complexes with unstructured or flexible regions. (92)

Cross-linking is based on a covalent linkage of two functional groups of the protein(s) of interest. The proteins are fragmented into peptides which are then separated by liquid chromatography (LC) and analyzed by mass spectrometry (MS). Peptides linked together constrain the distance between each other in the protein/complex. (92) The range of a cross-linker can be less than the maximum calculated distance,(93) but it is necessary to remember that it is impossible to cross-link the two interacting parts of the proteins because there is no space for the linker on the interaction interface so that surrounding areas are always cross-linked. (92)

There are two main approaches to MS analysis, the bottom-up approach and the top-down approach. The bottom-up approach was used in the experimental part of this thesis. First, the protein solution is mixed with the cross-linking reagent. Cross-linked and not cross-linked protein species can be separated by SDS-PAGE, single bands cut out and enzymatically digested. The peptides are then usually analyzed by LC-MS or LC-MS-MS. Finally, the cross-linked peptides are identified from the MS spectrum. (92)

There are many functional groups of cross-linking reagents. The most commonly used reagents are N-hydroxysuccinimides that react with amino groups of the lysine side chains and N-terminal amino groups of proteins (Figure 13). (92)

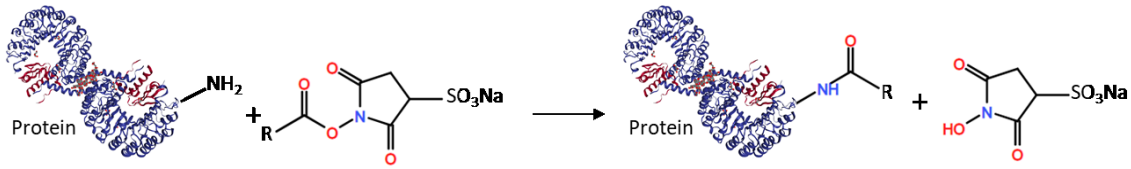

Figure 13 - Schematic reaction picture of protein cross-linked by N-hydroxysuccinimide

1.3.4. Hydrogen/Deuterium Exchange Connected with Mass Spectrometry

Hydrogen/deuterium exchange (HDX) analyzed by MS is a sensitive technique to study protein-solvent accessibility, membrane proteins, protein dynamics, protein-protein and protein-ligand interactions with relatively low resolution.(94, 95) This method is based on difference in hydrogen/deuterium exchange rate between amide groups of peptide bonds or side chains of amino acid residues and a deuterated solvent. Comparison of deuteration levels in different protein parts brings information about conformation and dynamics in the studied system. A lower deuteration rate in several consequential peptides shows a possible interaction interface in that area.

In most cases, the HDX is observed on the amides in the protein backbone as they are evenly distributed along the protein polypeptide chain and thus reflect the conformational dynamics of the proteins most comparably. Hydrogen atoms of the peptide bond amides form hydrogen bonds in and between secondary structure motifs of the protein so even a slight change of the conformation affects the HDX

rate. Moreover, the backbone amide hydrogens are exchanged in a measurable time rate at neutral pH depending on their exact local properties. A very important fact for the measurement is that the HDX rate of these amides is well quenchable at low pH and temperature.(96, 97) The lowest rate of HDX is at pH 2.5-3 and temperature below 0 °C. (94)

A peptide mapping is the first step of the experiment. The protein of interest is mixed with a low pH quenching solution, injected to LC where the protein is cleaved on a protease column, separated on a reverse-phase column, analyzed by MS-MS and the signals are assigned to peptides from the protein sequence. The goal of this procedure is to find combination of low pH quenching solution and the protease column leading to the best peptide coverage of the protein sequence. (94)

For the experiment, the protein of interest and its mixture with its interacting partner is diluted in a deuterated buffer. Then, the HDX is stopped at different time points by mixing with the quenching solution and freezing in liquid nitrogen. The samples are injected to LC-MS immediately after thawing. The signals are assigned to the peptides along with non-deuterated controls and analyzed automatically and manually. (94)

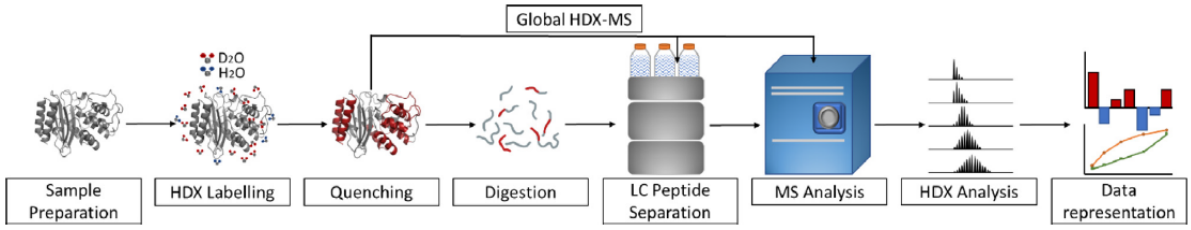

Figure 14 - Outline of HDX experiment (Taken from Oganesyan et al, 2018)

2. Research Aims

- Cloning of KIF5B variants
- Expression and purification of KIF5B and HDAC6 variants
- Determination of affinity between KIF5B and HDAC6 using microscale thermophoresis and surface plasmon resonance
- Specification of the structural aspects of KIF5B/HDAC6 interaction using hydrogen/deuterium exchange and chemical cross-linking coupled with mass spectrometry analysis

3. Materials and Methods

3.1. Materials

Acetic Acid	(Lachner, Czech Republic)
Acetonitrile	(Honeywell, Germany)
ACRYLAMIDE-BIS-ACRYL 37,5:1; 1 L	(M.G.P., Czech Republic)
Agarose	(Sigma-Aldrich Co., USA)
Agarose	(Sigma-Aldrich Co., USA)
AKTA Explore system	(GE Healthcare Life Sciences, USA)
Amicon® Ultra 0.4mL Filters for Protein Purification and Concentration	(Merck Millipore, Germany)
Ampicillin sodium salt	(Sigma-Aldrich Co., USA)
APS (3-(Cyclohexylamino)-1-propanesulfonic acid)	(Sigma-Aldrich Co., USA)
AscI	(New England Biolabs, USA)
Benzonase Nuclease	(Novagen, Germany)
BL21(DE3) pLysS Competent Cells	(Agilent, USA)
β-mercaptoethanol	(Sigma-Aldrich Co., USA)
Carbenicillin (Disodium Salt)	(ThermoFisher Scientific, USA)
cOmplete™, EDTA-free	(La Roche Ltd., Switzerland)
CutSmart Buffer	(New England Biolabs, USA)
Disuccinimidyl Glutarate	(Creative Molecules Inc. USA)
Disuccinimidyl Suberate	(Creative Molecules Inc. USA)
EDTA	(Sigma-Aldrich Co., USA)
ENrich™ SEC 70 10 x 300	(Bio-Rad, USA)
EX-CELL® 293 Serum-Free Medium for HEK 293 Cells	(Sigma-Aldrich Co., USA)
FastAP Thermosensitive Alkaline Phosphatase	(ThermoFisher Scientific, USA)
Fetal Bovine Serum	(Sigma-Aldrich Co., USA)
Formic acid	(Penta, Czech republic)
Gateway™ BP Clonase™ II Enzyme mix	(Invitrogen, USA)
Gateway™ LR Clonase™ II Enzyme mix	(Invitrogen, USA)
GelRed® Nucleic Acid Gel Stain	(Biotium, USA)
GenElute™ Gel Extraction Kit	(Sigma Aldrich Co., USA)
GenElute™ PCR Clean-Up Kit	(Sigma Aldrich Co., USA)

Gibco™ FreeStyle™ F17 Expression Medium	(Thermo Scientific, USA)
Glucose	(Duchefa, Netherlands)
glycerol	(MC Biomedical, USA)
Glycine	(Lachner, Czech Republic)
HaloTag® Biotin Ligand	(Promega, USA)
HEPES	(Sigma-Aldrich Co., USA)
High Five™ Cells	(Thermo Scientific, USA)
HisTrap HP, 5 ml	(GE Healthcare Life Sciences, USA)
HisTrap HP, 5 ml	(GE Healthcare Life Sciences, USA)
IGEPAL® CA-630	(Sigma-Aldrich Co., USA)
Imidazole	(SERVA Electrophoresis GmbH, Germany)
Insect-Xpress™ Protein-free Insect Cell Medium	(Lonza, Switzerland)
Kanamycin	(Sigma-Aldrich Co., USA)
KCl	(Lachner, Czech Republic)
LB Broth	(Sigma-Aldrich Co., USA)
Monolith NT.115 Capillaries	(NanoTemper, Germany)
NaCl	(Lachner, Czech Republic)
NotI	(New England Biolabs, USA)
NuPAGE 4–12% Bis–Tris gel	(Thermo Scientific, USA)
NuPAGE MES SDS running buffer	(Thermo Scientific, USA)
Orange G	(Sigma-Aldrich Co., USA)
PageRuler™ Prestained Protein Ladder	(ThermoFisher Scientific, USA)
Peptide microtrap column	(Optimize Technologies, USA)
Peristaltic Pump P-1	(GE Healthcare Life Sciences, USA)
PfuUltra II Hotstart PCR Master Mix	(Agilent, USA)
Polyethylenimine, Linear, MW 25000, Transfection Grade	(Polysciences, Inc., USA)
ProteOn™ GLM Sensor Chip	(Bio-Rad, USA)
ProteOn™ HTG Sensor Chip	(Bio-Rad, USA)
ProteOn™ NLC Sensor Chip	(Bio-Rad, USA)
QIAprep Spin Miniprep Kit	(Qiagen, USA)
QIAprep® Spin Miniprep Kit	(Quigen, Germany)
S.O.C. Ready-to-Use Medium	(Invitrogen, USA)
SDS	(Sigma-Aldrich Co., USA)
Sf9 cells in Sf-900™ III SFM Gibco™	(Thermo Scientific, USA)
Strep-Tactin® Suspension	(Iba, Germany)

Superose 6 Increase 10/300	(GE Healthcare Life Sciences, USA)
TCEP Hydrochloride	(AMRESCO, Ireland)
TEMED (N,N,N′,N′-Tetramethylethylenediamine)	(Sigma-Aldrich Co., USA)
Thiourea	(Sigma-Aldrich Co., USA)
Trizma® base	(Sigma-Aldrich Co., USA)
Tween20	(M.G.P., Czech Republic)
Urea	(Lachner, Czech Republic)
ZORBAX 300SB-C18 3.5 µm, 0.5 x 35 mm	(Agilent, USA)

3.2. Instruments

Monolith NT.115	(NanoTemper, Germany)
Avestin Emulsiflex C3	(ATA Scientific, Australia)
AKTA Explore system	(GE Healthcare Life Sciences, USA)
Bruker Daltonics 15T-Solarix XR FT-ICR mass spectrometer	(Bruker Corporation, Germany)
Agilent 1200 HPLC system	(Agilent Technologies, USA)
FPLC NGC™ Discover 10 Pro	(Bio-Rad, USA)
T100™ Thermal Cycler	(Bio-Rad, USA)
ProteOn™ XPR36 Surface Plasmon Resonance System	(Bio-Rad, USA)

3.3. Methods

3.3.1. PCR

The volume of each PCR was 20 µl. It was composed of a template DNA (1 ng/µl), a forward and reverse primer with the attB1 sequence at 5' ends (1µM) and 20-24 bases complementary to an amplified gene, 10 µl of DNA polymerase PfuUltra II Hotstart PCR Master Mix (Agilent, USA). The T100™ Thermal Cycler (Bio-Rad, USA) program was set according to the following protocol.

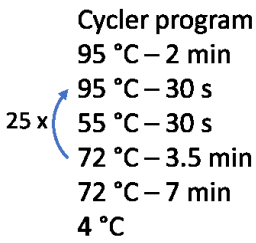

3.3.2. Agarose Gel DNA Electrophoresis

Orange G Solution: 0.2% Orange G, 20% (v/v) glycerol, 60mM EDTA, pH 8

TAE Buffer: 40mM Tris-HCl, 0.1% (v/v) acetic acid, 1mM EDTA, pH 8

DNA chain length was analyzed by DNA electrophoresis in agarose gel. 30 ng (1 µl) was mixed with 1 µl of Orange G solution and loaded to 0.8% agarose gel with GelRed® Nucleic Acid Gel Stain (Biotium, USA), run in the TAE Buffer at 90 V for 30 min. The results were observed under UV illumination.

3.3.3. Cloning

3.3.3.1. Gateway Cloning

Gateway technology uses BP and LR clonases to insert/swap pieces of DNA in between att sequences. The PCR product was inserted into a donor vector by BP reaction. The 8µl reaction mixture consisted of 100 ng of a PCR product, 100 ng of a destination plasmid and the 1.8 µl of Gateway™ BP Clonase™ II Enzyme mix (Invitrogen, USA). The mixture was incubated at room temperature overnight.

Analogically to the BP reaction, the LR reaction using the Gateway™ LR Clonase™ II Enzyme mix (Invitrogen, USA) was performed to insert the gene of interest into a suitable expression vector.

3.3.3.2. Cloning Using Restriction Endonucleases

Restriction endonucleases are enzymes that specifically recognise and cleave palindromic DNA sequences. Endonucleases NotI and AscI (New England Biolabs, USA) were used to digest the PCR products and the vectors. The products were assembled by T4 DNA ligase (ThermoFisher Scientific, USA).

3.3.4. Heat Shock Transformation of Plasmids into E. coli

1 µl (100 ng/µl) of the plasmid was mixed with 20 µl of Library Efficiency™ DH5α™ Competent Cells (Invitrogen, USA) and incubated on ice for 1 hour followed by a heat shock at 42 °C for 45 s and incubation on ice for 2 min. 200 µl of S.O.C. Ready-to-Use Medium (Invitrogen, USA) was added to the cells and incubated at 37 °C, 600 rpm, 1 h. The transformed cells were spread onto an LB agar plate with appropriate selection antibiotics (0.1 mg/ml) and incubated at 37 °C overnight.

3.3.5. DNA Isolation

Plasmid DNA was isolated from a 2ml overnight E. coli culture. The cell culture was centrifuged at 13000 g for 10 minutes. The recombinant DNA was isolated using QIAprep® Spin Miniprep Kit (Quigen, Germany) according to the manufacturer's protocol. The sequences were verified via Sanger sequencing (Eurofins, Germany).

3.3.6. Protein Expression

3.3.6.1. Protein Expression in E. coli

Resuspend buffer: 10 % (v/v) glycerol, 20mM Na_2HPO_4, 50mM NaCl, 1mM $MgCl_2$, pH 7.4

Expressions were carried out in BL21(DE3) pLysS Competent Cells (Agilent, USA). 100 ng of an expression plasmid was incubated with 15 µl of the competent cells on ice for 30 minutes. The transformation was performed as described in the previous chapter. 30 µl of the cell mixture was spread using glass beads on an LB agar plate with ampicillin (0.1 mg/ml, Sigma Aldrich Co., USA) and incubated at 37 °C overnight.

A single colony was transferred into 3 ml of LB medium with carbenicillin (0.1 mg/ml, ThermoFischer Scientific, USA) and 0.2% glucose and incubated at 220 rpm, 37 °C overnight. 2 l of LB medium in a 5l Erlenmeyer flask was infected by 1 ml of the overnight culture. After about 5 hours at optical density 0.6 (λ = 600 nm) the culture was transferred to 16 °C. After 1 hour, the expression was induced by 0.5mM IPTG and the culture was incubated overnight and then centrifuged at 5000 g for 15 min. The cell pellet was resuspended in 50 ml Resuspend Buffer with 1 tablet of protease inhibitors cOmplete™, EDTA-free (La Roche Ltd., Switzerland). The cells were lysed by four passages through Avestin C3 Emulsiflex (ATA Scientific, Australia) and centrifuged at 40000 g for 30 min.

3.3.6.2. Protein Expression in Baculovirus Expression System

A preparation of P1 generations of baculovirus was done by Régis Lemaitre from Max Planck Institute of Molecular Cell Biology and Genetics in Dresden, Germany. The P2 generation for expression was prepared by mixing 40 ml of Sf9 cells (10^6 cells/ml) in Insect-Xpress™ Protein-free Insect Cell Medium (Lonza, Switzerland), 800 µl of Fetal Bovine Serum (Sigma-Aldrich Co., USA) and 40 µl of the P1 generation. Cells were incubated at 27 °C, 110 rpm for 72-240 hours. Expression of a protein of interest was evaluated by SDS-PAGE every 24 hours. 200 µl of the cell culture was centrifuged at 500 g for 5 min, the cells were washed by resuspending in 500 µl of PBS, once more centrifuged at 500 g for 5 min and resuspended in 200 µl of the Sample Buffer and lysed at 95 °C, 5 min. 5 µl of samples were analyzed by SDS-PAGE. When the protein of interest was expressed, the cell culture was centrifuged for 10 min at 500 g. The supernatant was filtered through a 0.2µm pore size filter and stored at 4 °C.

For the expression, 5 ml of baculovirus P2 generation was added to 500 ml of High Five™ Cells (Thermo Scientific, USA) in Insect-Xpress™ Protein-free Insect Cell Medium (Lonza, Switzerland) at concentration 10^6 cells/ml in a 2l Erlemeyer flask and was incubated at 27 °C, 110 rpm for 72-120 hours. The expression was tested in the same way as described for P2 generation preparation. When the expression was visible, cells were harvested by centrifugation at 300 g for 10 min.

3.3.6.3. Protein Expression in HEK293/T17 Cells

Resuspend Buffer: 100mM Tris-HCl, pH 8.0, 10mM NaCl, 5mM KCl, 2mM $MgCl_2$, 10% (v/v) glycerol

Plasmids for expression in suspention HEK293/T17 cells were already cloned via Gateway Cloning System as published before (98) with N-terminal tags (Twin-Strep-Halo-GFP-tag, His-Twin-Strap-HALO-tag, Twin-Strep-FLAG-HALO-tag) with the CMV promoter and the TEV site for the removal of the tags.

0.7 mg of an expression plasmid in 17.5 ml of PBS and 2.1 ml of linear polyethyleneimine (1mg/ml, Polysciences, Inc., USA) were mixed and added to 350 ml of the cell culture (4 x 10^6 cells/ml) in the Gibco™ FreeStyle™ F17 Expression Medium (Thermo Scientific, USA) in a 2l Erlenmeyer flask at 37 °C, 110 rpm, 5% CO_2. After 4 hours, 350 ml of EX-CELL® 293 Serum-Free Medium (Sigma-Aldrich Co., USA) was added to the cell culture and incubated for 48-96 h under the same conditions. Protein expression was monitored by SDS-PAGE. Cells were harvested by centrifugation at 500 g, 4 °C, 5 min.

The cell pellet was resuspended in 30 ml of the Resuspend Buffer. 3 µl of Benzonase Nuclease (Novagen, Germany) and 1 tablet of protease inhibitors cOmplete™, EDTA-free (La Roche Ltd., Switzerland) were added to the cells. The cell suspension was sonicated three times at 15 W, 20 s. Igepal CA-630 (Sigma-Aldrich Co., USA) was added to a final concentration of 0.2% (v/v) and the mixture was incubated on ice for 20 min. NaCl was added to final concentration of 150mM. After another 20min incubation on ice, the mixture was centrifuged at 9000 g, 4 °C, 15 min. The supernatant was harvested and centrifuged 30 000 g, 4 °C, 15 min, and ready for purification.

3.3.7. Affinity Chromatography

3.3.7.1. NiNTA Affinity Chromatography of Proteins Expressed in E. coli

Buffer A: 50mM Na_2HPO_4, 400mM NaCl, 30mM imidazole, 10% (v/v) glycerol, pH 7.4

Buffer B: 50mM Na_2HP0_4, 100mM NaCl, 500mM imidazole, 10% (v/v) glycerol, pH 7.4

NiNTA affinity chromatography uses Ni^{2+} complexed in NTA which binds the His-tag, a peptide composed of several successive histidine residues (usually six to twelve) to separate a His-tagged protein from the cell lysate. When the majority of contaminating proteins is washed away, the His-tagged protein is eluted from the column by excess of imidazole, but it can also be eluted by a low pH or protease digestion of the His-tag.

The supernatant from centrifugation after lysis was injected onto HisTrap HP, 5 ml (GE Healthcare Bio-Sciences, USA) connected to FPLC NGC™ Discover 10 Pro (Bio-Rad, USA). The flow rate was 3.5 ml/min. After injection, the column was washed with 60 ml of Buffer A. The His-tagged protein was eluted by a 0 to 100 % linear gradient of Buffer B in 50 ml. 4ml fractions were collected and resolved by SDS-PAGE to visualize results of purification. The tags were cleaved by the TEV protease at the 1:4 (w/w) ratio of TEV:purified protein at 4 °C overnight. After 10-fold dilution by the Buffer A (with no imidazole), the mixture was injected to the NiNTA column, and the protein was collected in the flow through fraction.

3.3.7.2. NiNTA Affinity Chromatography of Proteins Expressed in Baculovirus Expression System

Lysis Buffer: 50mM Na_2HPO_4, 5% (v/v) glycerol, 300mM KCl, 1mM $MgCl_2$, 0.1% (v/v) Tween20, 10mM β-mercaptoethanol, 0.1mM ATP, 30mM imidazole, protease inhibitors, 0.5% (v/v) triton, pH 7.5

Wash Buffer I: 50mM Na_2HPO_4, 5% (v/v) glycerol, 300mM KCl, 1mM $MgCl_2$, 0.1% (v/v) Tween20, 10mM β-mercaptoethanol, 0.1mM ATP, 30mM imidazole, pH 7.5

Wash Buffer II: 50mM Na_2HPO_4, 5% (v/v) glycerol, 300mM KCl, 1mM $MgCl_2$, 0.1% (v/v) Tween20, 10mM β-mercaptoethanol, 0.1mM ATP, 30mM imidazole, 700mM NaCl, pH 7.5

Elution Buffer I: 50mM Na_2HPO_4, 5% (v/v) glycerol, 300mM KCl, 1mM $MgCl_2$, 0.1% (v/v) Tween20, 10mM β-mercaptoethanol, 0.1mM ATP, 100mM imidazole, pH 7.5

Elution Buffer II: 50mM Na_2HPO_4, 5% (v/v) glycerol, 300mM KCl, 1mM $MgCl_2$, 0.1% (v/v) Tween20, 10mM β-mercaptoethanol, 0.1mM ATP, 200mM imidazole, pH 7.5

Elution Buffer III: 50mM Na_2HPO_4, 5% (v/v) glycerol, 300mM KCl, 1mM $MgCl_2$, 0.1% (v/v) Tween20, 10mM β-mercaptoethanol, 0.1mM ATP, 300mM imidazole, pH 7.5

Cells were resuspended in 30ml of the Lysis Buffer and centrifuged at 40 000 g, 4 °C, 2 h. The supernatant was harvested and mixed with 15 µl of Benzonase Nuclease (Novagen, Germany). The mixture was injected to HisTrap HP, 5 ml (GE Healthcare Life Sciences, USA) connected to a P-1 Peristaltic Pump (GE Healthcare Life Sciences, USA) at flow rate 3.5 ml/min preequilibrated by the Wash Buffer I. After the injection, the column was washed by 15 ml of each Wash Buffer I/Wash Buffer II/Wash Buffer I. The protein was eluted by 15 ml of each Elution Buffer I/ Elution Buffer II/Elution

Buffer III. All fractions were collected and analyzed by SDS-PAGE. The tags were cleaved by the C3 protease at the 1:13 (w/w) ratio of the TEV:purified protein.

3.3.7.3. Strep-Tactin Affinity Chromatography of Proteins Expressed in HEK293/T17 Cells

Equilibration Buffer: 100mM Tris-HCl, 150mM NaCl, 5mM KCl, 2mM $MgCl_2$, 10% glycerol, pH 8.0

Elution Buffer: 50mM Tris-HCl, 150mM NaCl, 10mM KCl, 10% glycerol, 3mM desthiobiotin, pH 8.0

Wash Buffer: 100mM Tris-HCl, 100mM NaCl, pH 10.2

In this affinity chromatography, a streptavidin recombinant derivative is covalently bound to resin beads. The recombinant protein of interest binds to Strep-Tactin via its Strep-tag. The protein is eluted by desthiobiotin.

4 ml of Strep-Tactin® Suspension (Iba, Germany) in a gravity-flow column was washed with the Equilibration Buffer. The supernatant from HEK293-T17 cells was injected onto the column and it was washed by 7 ml of the Wash Buffer. The column was incubated with 7 ml of the Wash Buffer with 3mM ATP and 10mM $MgCl_2$ for 15 min. The column was washed with 7 ml of the Wash Buffer once more. The protein was eluted with 20 ml of the Elution Buffer. All fractions were collected and analyzed by SDS-PAGE.

The tags were cleaved by the TEV protease at the 1:15 ratio (w/w) of TEV:purified protein if required. The protein was dialysed in 2l of the Equilibration Buffer and injected to the Strep-Tactin column, and the protein was collected in the flow through fraction.

3.3.8. SDS-PAGE

Sample Buffer: 250mM Tris-HCl, 10% (w/w) SDS, 30% (v/v) glycerol, 0,75mM β-mercaptoethanol, 0.3mM Bromphenol blue, pH 6.8

Running Buffer: 25mM Tris-HCl, 200mM glycine, 0.1% (w/w) SDS

Coomassie Brilliant Blue Dye: 50 mg/l Brilliant Blue G, 3 ml/l acetic acid

Focusing Gel: 5% (w/w) acrylamide-bis-acryl 37,5:1, 0.1% (w/w) APS, 0.1% (v/v) TEMED, 125mM Tris-HCl, 0.1% (w/w) SDS, pH 6,8

Resolving Gel: 10-17.5% (w/w) acrylamide-bis-acryl 37,5:1, 0.1% (w/w) APS, 0.1% (v/v) TEMED, 125mM Tris-HCl, 0.1% (w/w) SDS, pH 8.8

Analysed samples were mixed with a Sample Buffer at the 4:1 ratio. The samples were heated to 95 °C for 5 minutes. Sample were loaded to each well of the gel. 1 µl of PageRuler™ Prestained Protein Ladder (ThermoFisher Scientific, USA) was loaded to one well as a standard of molecular weights. Proteins

were separated at 150 V for 1.5 hour. The gel was stained by the Coomassie Brilliant Blue Dye in a microwave for 1 min, at room temperature for 15 min and then destained in deionised water.

3.3.9. Size Exclusion Chromatography

Size exclusion chromatography (SEC) separates particles by their size. Particles migrate through the column and are slowed down by entering the resin pores if they fit into them. Bigger particles cannot enter the pores so that they migrate faster than the smaller ones.

3.3.9.1. Size Exclusion Chromatography of Protein Expressed in E. coli and Baculovirus Expression System

SEC Buffer: 10mM Na_2HPO_4, 137mM NaCl, 1.8mM KH_2PO_4, 2.7mM KCl, 0.1mM ATP, 1mM $MgCl_2$, pH 7.4

Proteins purified by affinity chromatography were concentrated to 0.5 ml in Amicon® Ultra 4mL Filters (Merck Millipore, Germany) and injected onto a SEC column [ENrich™ SEC 70 10 x 300 (Bio-Rad, USA) for constructs up to 70 kDa, Superose 6 Increase 10/300 (GE Healthcare Bio-Sciences, USA) for proteins bigger than 70 kDa] equilibrated in the SEC Buffer. Columns were connected to NGC™ Discover 10 Pro (Bio-Rad, USA) and the flow was 0.5-1ml/min. 0.5ml fractions were collected and analyzed by SDS-PAGE.

3.3.9.2. Size Exclusion Chromatography of Proteins Expressed in HEK293/T17 Cells

SEC Buffer: 30mM HEPES, 140mM NaCl, 10mM KCl, 3% (v/v) glycerol, 0.25mM TCEP, pH 7.4

Proteins purified by affinity chromatography were concentrated to 4 ml in Amicon® Ultra 4mL Filters (Merck Millipore, Germany) and injected on a SEC column Superose 6 10/300 (GE Healthcare Bio-Sciences, USA) equilibrated in the SEC Buffer. The column was connected to the AKTA Explore system (GE Healthcare Life Sciences, USA) and the flow rate was 1.5 ml/min. 0.5ml fractions were collected and analyzed by SDS-PAGE.

3.3.10. Hydrogen/Deuterium Exchange Connected with Mass Spectrometry

3.3.10.1. Mapping

Running Solution A: 2% (v/v) acetonitrile, 0.4% (v/v) formic acid

Running Solution B: 95% (v/v) acetonitrile, 0.4% (v/v) formic acid

For a mapping experiment, 300 pmol of a protein in 50 µl was used. The sample was mixed with 50 µl of a quencher solution (1M glycine, 4M urea and 6M thiourea, pH 2.3) and the mixture injected into an

HPLC-MS/MS system [Agilent 1200 HPLC (Agilent Technologies, USA), the Bruker Daltonics 15T-Solarix XR FT-ICR mass spectrometer (Bruker Corporation, Germany)] with a variable flow (100-600 µl/min) through a protease column (66 µl bed volume, pepsin, nepenthesin 1, nepenthesin 2, spergillopepsin, rhizopuspepsin). Peptides from the digestion were desalted online on a Peptide microtrap column (Optimize Technologies, USA) and separated on a reversed phase column ZORBAX 300SB-C18 3.5µm, 0.5 x 35 mm (Agilent, USA) using a linear gradient 10-45 % of Running Solution B in 20 min. Injection and switching valves and columns were placed in an ice box to minimize the back-exchange. The coverage of a protein sequence from MS/MS spectra was analyzed by MASCOT containing the sequence of the proteins of interest.

3.3.10.2. HDX Experiment

Reaction Buffer: 50mM HEPES, 140mM NaCl, 10mM KCl, 3% (v/v) glycerol, 1mM TCEP, 0.1mM ATP pH 7.4 in H_2O/D_2O

In HDX experiment, a free target protein and its complex with its binding partner together with non-deuterated controls, were used. The HDX was initiated by 10-fold dilution of the proteins by the deuterated reaction buffer. 100 pmol of the protein of interest was in one sample. For the complex sample, 100 pmol of the protein of interest was mixed with 400 pmol of the binding partner. After incubation with the D_2O Reaction Buffer at the 1:9 ratio, the HDX was stopped by vortexing the reaction mixture with 50 µl of a quencher (1M glycine, pH 2.3, or 1M glycine, 4M urea, 6M thiourea, pH 2.3) and fast freezing in liquid nitrogen. The deuteration was stopped at four time point (20 s, 2 min, 20 min, 2h).

Each sample was thawed just before injection to the Agilent 1200 HPLC system (Agilent Technologies, USA). The sample was digested online in a 66µl bed volume protease column, desalted on a Peptide microtrap column (Optimize Technologies, USA), separated on a reversed phase column ZORBAX 300SB-C18 3.5µm, 0.5 x 35 mm (Agilent, USA) and analyzed at the Bruker Daltonics 15T-Solarix XR FT-ICR mass spectrometer (Bruker Corporation, Germany). Spectra of partially deuterated peptides were processed by Data Analysis 4.2 (Bruker Daltonics, Billerica, MA) and by an in-house program called DeutEx.

3.3.11. Chemical Cross-linking Connected with Mass Spectrometry

Reaction buffer: 20mM HEPES, 140mM NaCl, 10mM KCl, 1mM TCEP, pH 7.4

Sample Buffer: 250mM Tris-HCl, 10% (w/w) SDS, 30% (v/v) glycerol, 0,75mM β-mercaptoethanol, 0.3mM Bromphenol blue, pH 6.8

Running Solution A: 2% (v/v) acetonitrile, 0.4% (v/v) formic acid

Running Solution B: 95% (v/v) acetonitrile, 0.4% (v/v) formic acid

Cross-linking experiments were performed for individual proteins of interest as well as their mixtures. Concentration of each protein in each reaction was 1.4 mg/ml in the Reaction Buffer. After five minutes at room temperature, 50x molar excess of disuccinimidyl suberate (DSS) or disuccinimidyl glutarate (DSG), cross-linking reagents freshly dissolved in DMSO was added to the final volume of 20 µl. The reactions were incubated at room temperature for 30 minutes. Cross-linked samples were mixed with the Sample Buffer and separated in a NuPAGE 4–12% Bis–Tris gel (Thermo Scientific, USA) using NuPAGE MES SDS running buffer (Thermo Scientific, USA). The cross-linked proteins were digested by trypsin at the 1:20 mass ratio at 37 °C overnight.

Peptides extracted from the gel as well as peptides cleaved in solution were loaded on a trap column ZORBAX 300SB-C18, 5um, 5x0.3mm (Agilent, USA) and desalted for 5 min at the flow rate of 20 µl/min. Peptides were then separated by ZORBAX SB C18 RR 3.5µm 150 x 0.3 mm (Agilent, USA) at a flow rate 10 µl/min using a capillary HPLC system (Agilent, USA) under the following gradient of the Running Solution B: 1–10% in 1 min, 10–45% B in 19 min, 45–95% B in 5 min. The column was heated to 50 °C and connected directly to the Bruker Daltonics 15T-Solarix XR FT-ICR mass spectrometer (Bruker Corporation, Germany). Data processing was performed by DataAnalysis 4.2 (Bruker Corporation, Germany). The cross-linked peptides were identified using the Automated Spectrum Assignment Program.(99)

3.3.12. Microscale Thermophoresis

MST buffer: 50mM NaCl, 50mM Na_2HPO_4, 10% (v/v) glycerol, 0.1% (v/v) Tween20, 1 mg/ml BSA, pH 7.4

Two-fold dilution series in the final volume of 10 µl were prepared from a non-labelled protein in the MST buffer. A GFP-labelled protein was diluted in the MST buffer to final concentration of 200nM. 10 µl of the GFP-labelled protein was mixed with each concentration of the non-labelled protein. The reactions were incubated at room temperature for 5 minutes. Reactions were centrifuged at 12000 g for 5 min. Then, the reactions were transferred into Monolith NT.115 Capillaries (NanoTemper, Germany). The capillaries were inserted into Monolith NT.115 (NanoTemper, Germany). Excitation power was set to 60 %, MST power was set to 40 %. First, a Cap Scan was done to confirm the fluorescence intensity. Second the MST experiment was run for every capillary with 5 s of only excitation power, 20 s of both laser powers on, and last 5 s with only excitation power on. The results were processed with MO.Control v1.6 and GraphPad Prism.

3.3.13. Surface Plasmon Resonance

3.3.13.1. GLM Sensor Chip

Phosphate Running Buffer: 50mM Na_2HPO_4, 50mM NaCl, 5/10% (v/v) glycerol, 0.005% (v/v) Tween20

HEPES Running Buffer: 30mM HEPES, 140mM NaCl, 30mM KCl, 3% (v/v) glycerol, 0.5mM $MgCl_2$, 1mM TCEP, 0.05% (v/v) Tween20

A ProteOn™ GLM Sensor Chip (Bio-Rad, USA) was preconditioned by 30µl injections of 0.5% SDS, 50mM NaOH and 50mM HCl with a flow rate of 30 µl/min. Activation of the chip surface was performed by a 150µl injection of 200mM EDAC and 50mM Sulfo-NHC, which were mixed immediately before the injection, with a flow rate of 30 µl/min. A ligand was diluted in 10mM sodium acetate, 10mM NaCl, 0.005% Tween20, pH 4.5, to concentration 20 µg/ml and 300 µl was injected to the chip with a flow rate of 30 µl/min. The free active sites on the chip were blocked by injection of 150 µl of 1M ethanolamine.

After 100µl Running Buffer flush of the chip with a flow rate of 100 µl/min, a 3-fold dilution series of analytes were prepared and 100 µl injected to the chip with a flow rate of 40 µl/min and dissociation time 600 s. The chip was regenerated with 30 µl of 10mM glycine, pH 2, with a flow rate of 100 µl/min.

3.3.13.2. NLC Sensor Chip

A ProteOn™ NLC Sensor Chip (Bio-Rad, USA) was preconditioned by 30µl injections of 0.5% SDS, 50mM NaOH, 100mM HCl and 50mM NaOH. After flushing with the Running Buffer, a biotinyated ligand (20 µg/ml) was injected at the chip with a flow rate of 30 µl/min. (The prepare a biotin labelled protein, 5 mg of a HALO-tagged protein was mixed 10 µl of HaloTag® Biotin Ligand (Promega, USA) and incubated at 4 °C overnight.) The injection was stopped when the signal reached 400 RU.

After a 100µl flush by a Running Buffer with a flow rate of 100 µl/min, 200 µl of different dilutions of an analyte were injected to the chip with a flow rate of 50 µl/min and a dissociation time 600 s. The chip was regenerated with 30 µl of 1M NaCl with a flow rate of 100 µl/min.

3.3.13.3. HTG Sensor Chip

A ProteOn™ HTG Sensor Chip (Bio-Rad, USA) was preconditioned with 30µl injections of 0.5% SDS, 50mM NaOH, 100mM HCl, 300mM EDTA, pH 8, with a flow rate of 30 µl/min. The chip was activated

by 10mM solution of $NiSO_4$ (150 µl, 30 µl/min). After 100µl flush of a Running Buffer, a His-tagged ligand (20 µg/ml) was immobilized at the chip (25 µl, 30µl/min).

After 100µl flush of a Running Buffer, a dilution series of an analyte was injected to the chip (100 µl, 50 µl/min) with a 1200s dissociation time. The chip was regenerated with 300mM EDTA (25 µl, 100 µl/min), 100mM HCl (30 µl, 100 µl/min) and reactivated with 10mM solution of $NiSO_4$ (150 µl, 30 µl/min).

4. Results

There is limited structural information concerning the interaction interface between human kinesin-1 (KIF5B) and its protein activators and/or adaptors. At the same time, the C-terminal part is the most likely implicated in these interactions as have been described in some cases (Chapter 1.2.3).(51, 71) The aim of this diploma thesis is to analyze interactions between human HDAC6 and KIF5B. To this end, we designed, expressed and purified different constructs of KIF5B as well as HDAC6 and mapped their interactions using an array of biophysical approaches.

4.1. Cloning of KIF5B Constructs

Several constructs of KIF5B have been designed and cloned into expression plasmids (Table 1). The DNA sequence encoding human KIF5B (UniProtKB - P33176) was used as a template for all KIF5B constructs.

Table 1 - List of KIF5B constructs

Construct length (AA)	Description	Expression system	Schematic picture
1-963	Full-length	Baculovirus	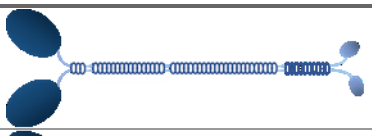
1-905	Not autoinhibited	Baculovirus	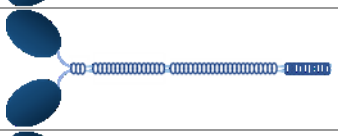
1-824	Not autoinhibited, no coiled-coil 3	Baculovirus	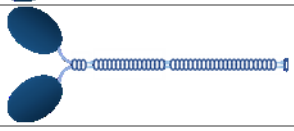
822-906	Coiled-coil 3	*E. coli*	
889-963	Tail	*E. coli*	

Three constructs comprising the motor domain (KIF5B 1-963, KIF5B 1-905, KIF5B 1-824) were cloned into plasmids for baculovirus expression. A DNA sequence for each construct was amplified by PCR. The PCR product was digested by NotI and AscI restrictases to create complementary ends for ligation to the expression vector (Figure 15). The DNA sequence encoding KIF5B variants were ligated into the

vectors using T4 DNA ligase. Figure 16 shows a scheme of an expression plasmid. The plasmid sequence was verified by Sanger sequencing (Eurofins, Germany).

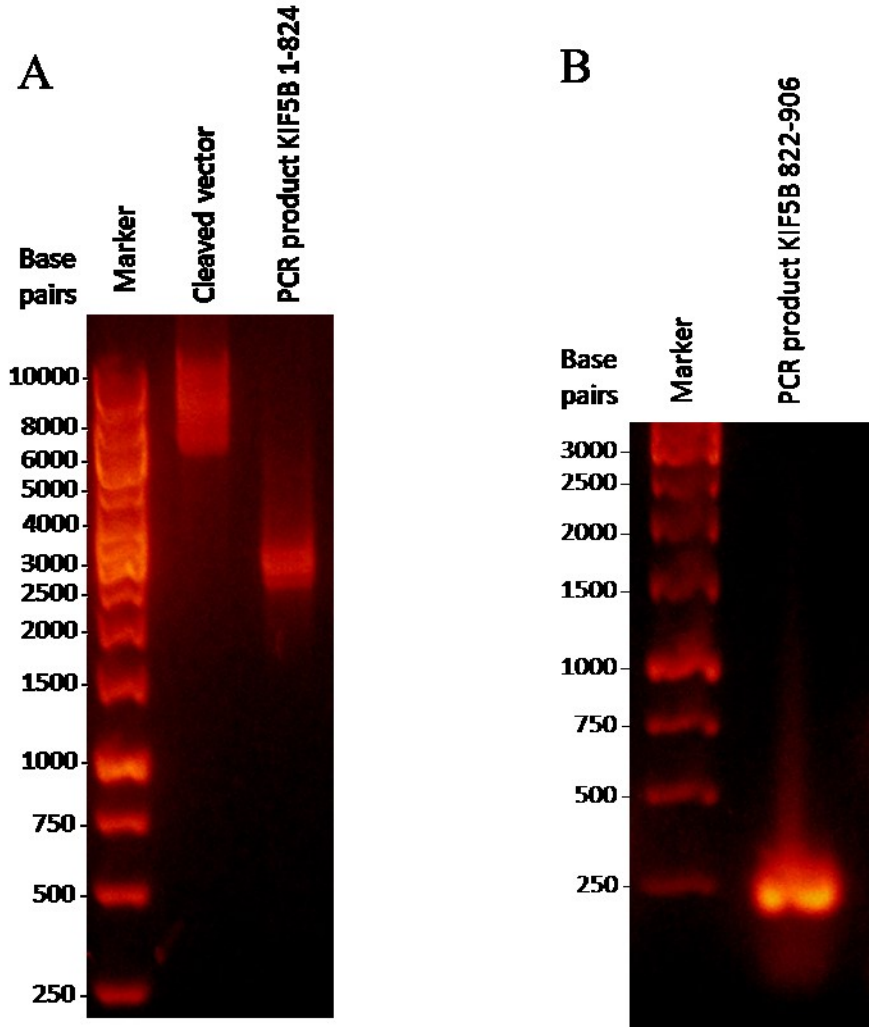

*Figure 15 – **A** An agarose gel of the digested vector (5000 bp) and the digested PCR product of the KIF5B 1-824 construct (2500 bp), **B** An agarose gel of the PCR product of the KIF5B 822-906 construct (250 bp)*

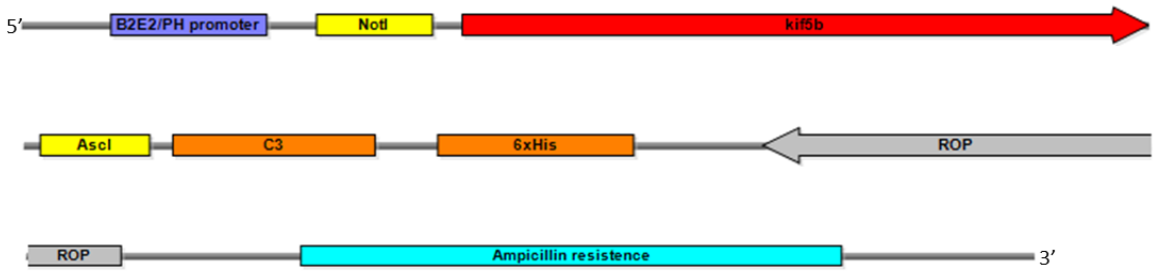

Figure 16 - Scheme of a plasmid for KIF5B expression in baculovirus expression system

The expression plasmid comprises a sequence encoding a KIF5B variant, NotI and AscI restriction sites, the B2E2/PH promotor driving expression in High Five™ cells, the His-tag (His-GFP) sequence, a sequence for digestion of a tag by C3 protease, the ROP sequence for the plasmid replication and an ampicillin resistance. Linearized representation of the circular vector shown.

KIF5B constructs comprising the C-terminus (KIF5B 822-906 and KIF5B 889-963) were cloned into plasmids for expression in *E. coli* using Gateway technology. The coding DNA sequences were amplified by PCR (Figure 15). Using BP clonase, the PCR products were inserted into a pD221 donor vector and the construct identity verified by Sanger sequencing (Eurofins, Germany). Next, the coding sequences were inserted into the destination vectors using LR clonase. Figure 17 shows a scheme of the expression plasmid.

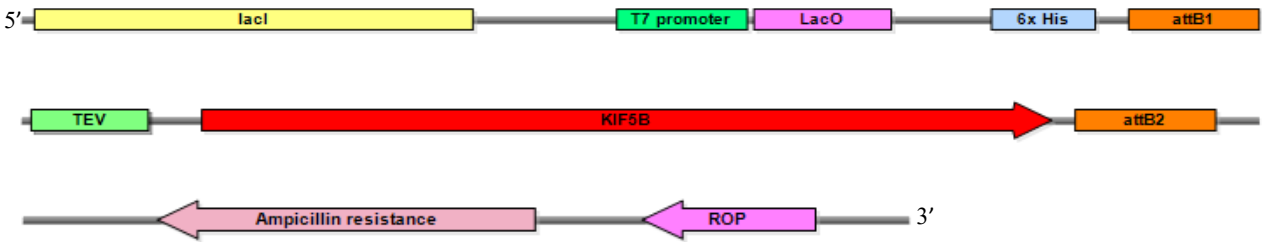

Figure 17 - Scheme of a plasmid for KIF5B expresstion in E.coli

The expression plasmid comprising a sequence encoding a KIF5B variant, LacI for lactose repressor, lacO for lactose operon, attB sites for Gateway LR clonase, ROP sequence for plasmid replication, the T7 promotor for T7 RNA polymerase, the His-tag coding sequence, a sequence for digestion of the tag by TEV protease and an ampicillin resistance. Linearized representation of the circular vector shown.

4.2. Purification

4.2.1. HDAC6 Constructs

4.2.1.1. Strep-Tactin Affinity Chromatography

HDAC6 constructs comprising the Twin-Strep-tag or Twin-Strep-GFP-tag were expressed in HEK293/T17 cells (Table 2). Cells were transiently transfected by expression plasmids, harvested three days post-transfection and the cell pellet lysed in a lysis buffer. The clarified cell lysate was injected onto a Strep-Tactin column. N-terminally tagged HDAC6 variants were eluted by a buffer containing 3mM desthiobiotin and analyzed by SDS-PAGE (Figure 18, a representative gel of HDAC6 FL purification). This single purification step was successful and provided the protein of interest with purity >90 % as estimated from the gel.

Table 2 - List of HDAC6 constructs

Construct length (AA)	Description	Schematic picture
1-1215	Full-length	
GFP-1-1215	Full-length	
GFP-1-855	N-terminus, DD1 and DD2	
GFP-844-1112	SE14 domain	

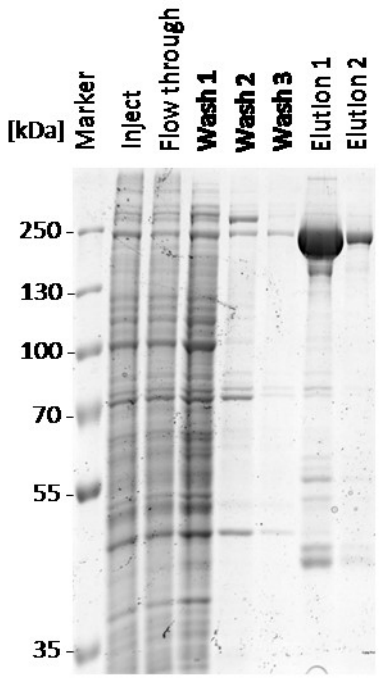

Figure 18 – SDS-PAGE analysis of a Strep-Tactin purification step of HDAC6 FL (176 kDa)

4.2.1.2. Size Exclusion Chromatography

A final step of HDAC6 purification was size exclusion chromatography which separates the protein of interest from its aggregates, cleaved tags and contaminating proteins of a different size. The protein was concentrated to 0.5ml and injected onto a Superose 6 10/300 size exclusion column. The SEC run process was monitored by measuring absorbance at 280 nm in time and the resulting chromatogram of

HDAC6 FL is shown in Figure 19. 0.5ml fractions were collected from the column and samples from these fractions were loaded onto polyacrylamide gel (Figure 20). Fractions 13-16 were frozen in liquid nitrogen and stored in -80 °C. The final yield of a pure HDAC6 construct is about 2 mg per 1 l of the HEK293/T17 cell culture.

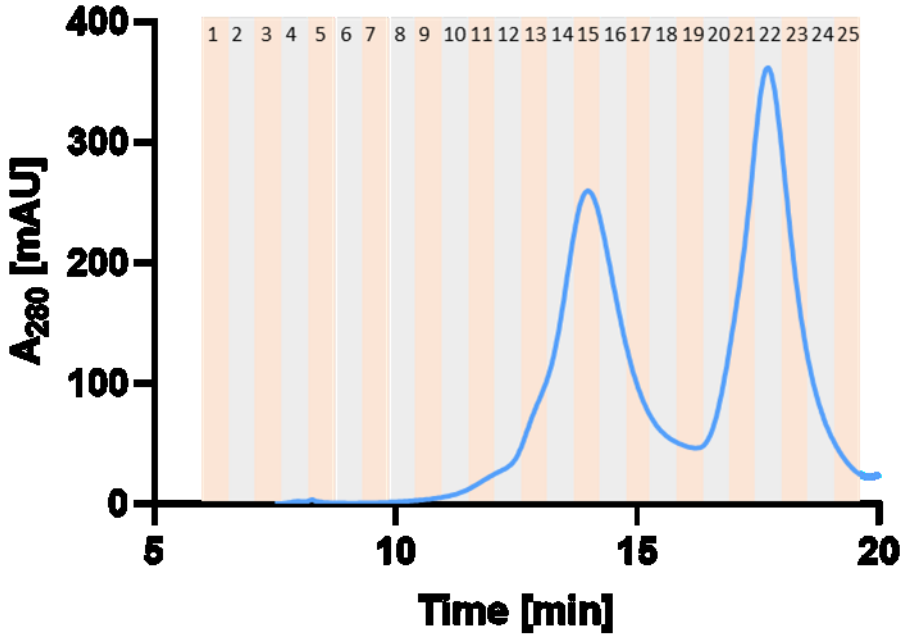

Figure 19 - A chromatogram of HDAC6 FL purification using Superose 6 10/300

The first peak corresponds to HDAC6 FL, the second peak belong to the cleaved tag.

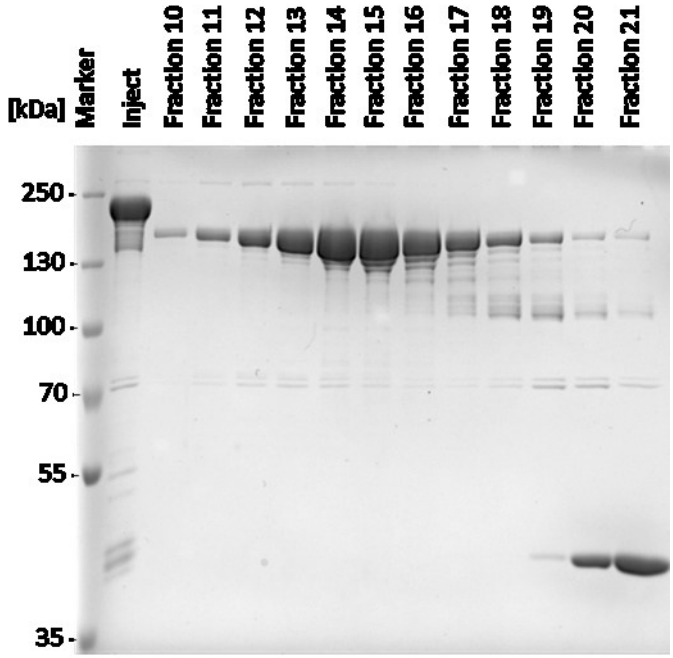

Figure 20 - SDS-PAGE analysis of HDAC6 FL (131 kDa) fractions corresponding to the chromatogram in Figure 19

4.2.2. KIF5B Constructs

4.2.2.1. NiNTA Chromatography

NiNTA affinity chromatography was used to purify His-tagged KIF5B constructs from cell lysate. The lysate was injected onto the column, washed and eluted by either linear 0 – 500mM (*E. coli* expression) or a step-wise 100mM, 200mM and 300mM (baculovirus expression) imidazole gradient. The results of purification were analyzed by SDS-PAGE (Figure 21). Elution fractions 6-14 and 1-3 from figure 21 and 22., respectively were concentrated and purified by the next purification step. The affinity chromatography was successful and provided the protein of interest with high purity as a majority of the contaminating proteins was washed out.

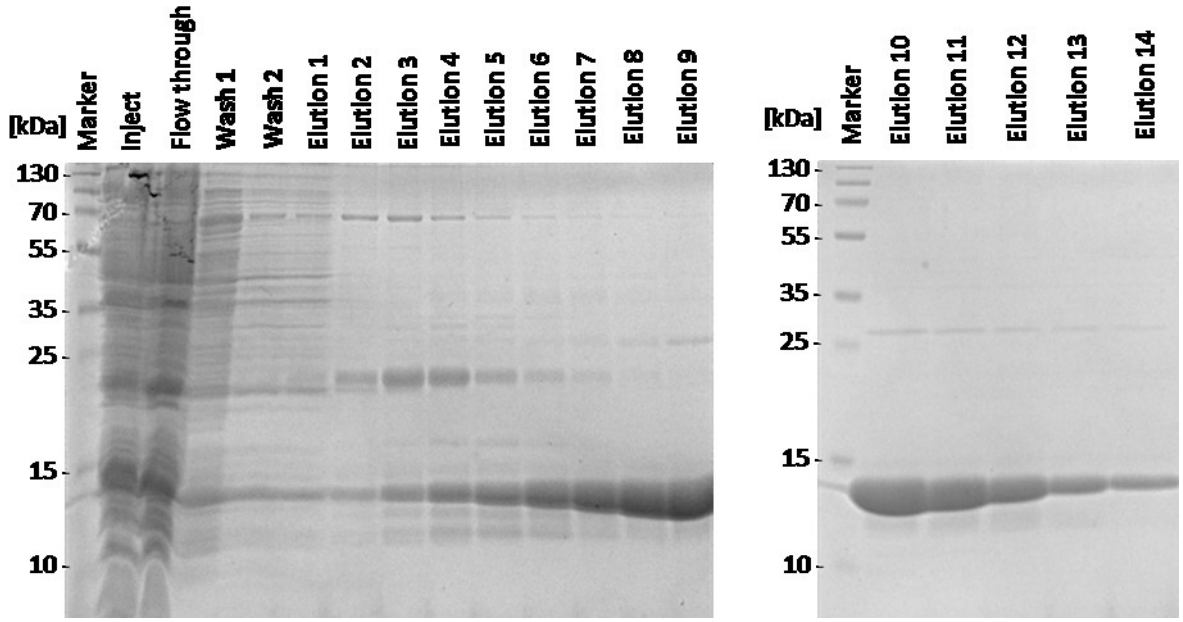

Figure 21 - Fraction from NiNTA affinity chromatography of KIF5B 822-906 (14 kDa) analyzed by SDS-PAGE

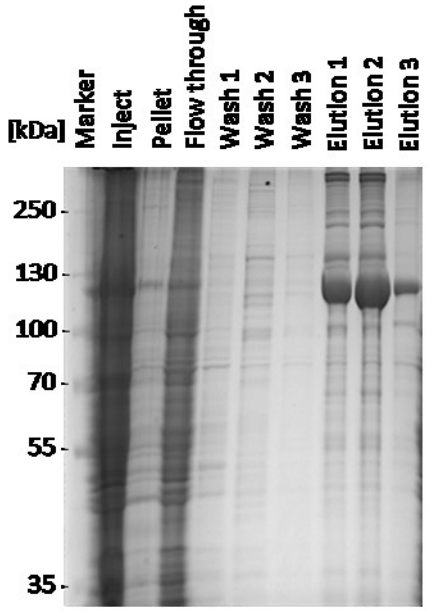

Figure 22 – Fractions from the NiNTA affinity chromatography of KIF5B FL (112 kDa) analyzed by SDS-PAGE

4.2.2.2. Size Exclusion Chromatography

Size exclusion chromatography was used as a final purification step for KIF5B constructs to separate the protein from aggregates and contaminating proteins. The SEC run process was monitored by measuring absorbance at 280 nm in time and the resulting representative chromatograms are shown in Figure 23. The Enrich 70 10/300 column was used for the KIF5B constructs (*E. coli* expression). Fractions 3-5 were frozen in liquid nitrogen and stored at -80 °C. An average yield of the protein was 3.5 mg of pure protein per 1 l of the *E. coli* culture. The Superose 6 10/300 column was used for the N-

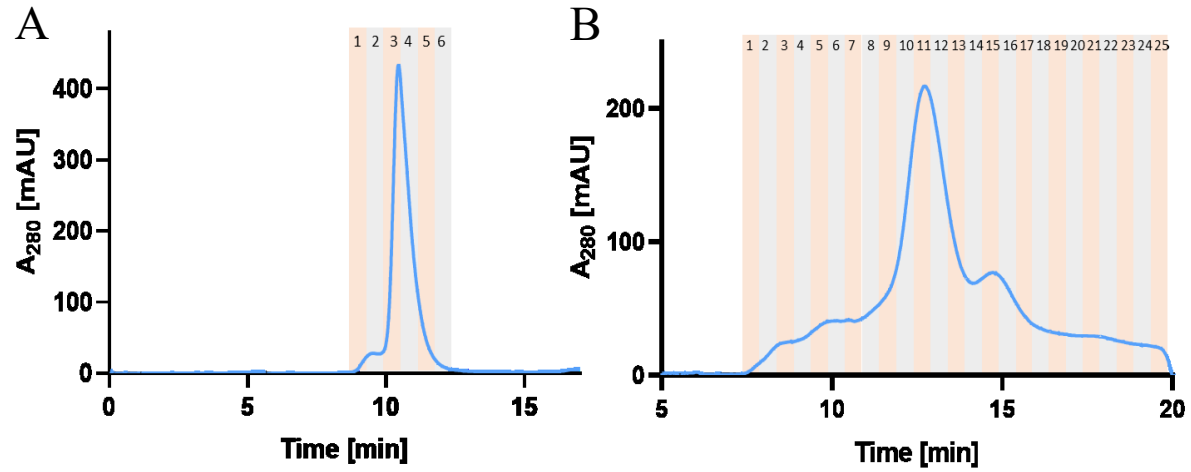

Figure 23 – Chromatograms from SEC

***A** KIF5B 822-906 chromatogram from column Enrich 70 10/300, **B** KIF5B FL chromatogram from column Superose 6 10/300, samples from each fraction were an alyzed at SDS-PAGE (Figure 24)*

terminal KIF5B constructs (baculovirus expression). Fractions 10-13 were frozen in liquid nitrogen and stored -80 °C. An average yield was 1.2 mg of a protein per 1 l of the High Five Cell culture.

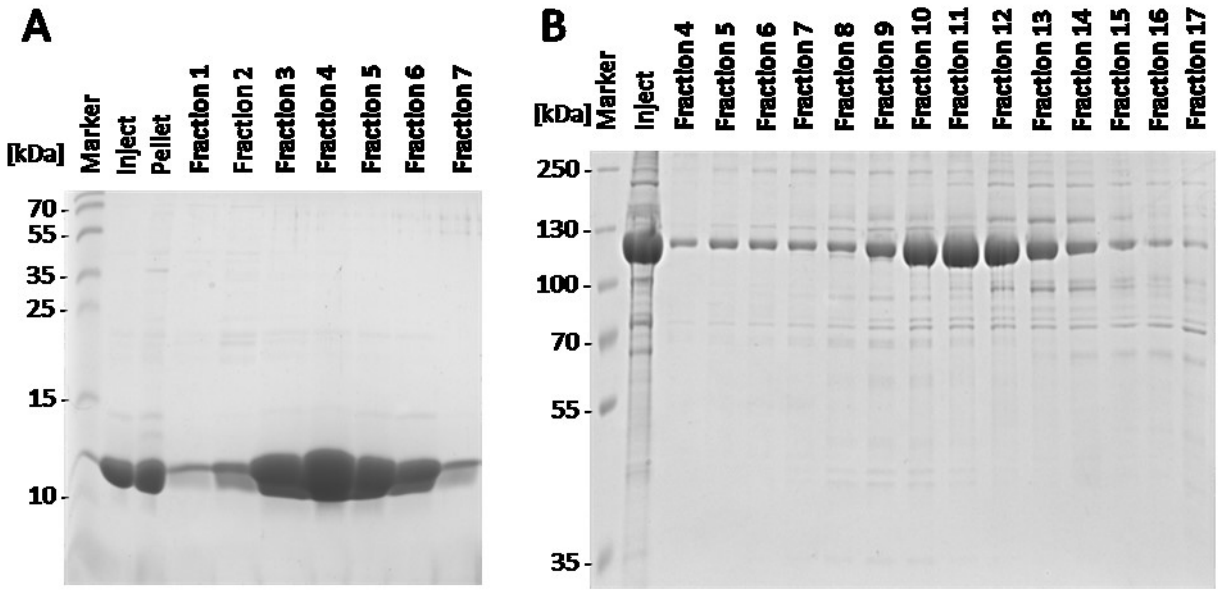

*Figure 24 – SDS-PAGE analysis of SEC fractions of KIF5B 822-906 (10 kDa, **A**) and KIF5B FL (110 kDa, **B**)*

4.2.3. Purification Results

All the purified constructs were loaded into polyacrylamide gels (Figure 25). The gels show that all constructs were successfully expressed and purified. For the KIF5B 889-963 construct, two bands are visible in the SDS-PAGE gel. Using LC-MS/MS, we determined that the lower molecular weight species is the construct truncated by 16 amino acids at the C-terminus (data not shown). This construct was thus used as a mixture of the two different lengths of 889-963 and 889-947.

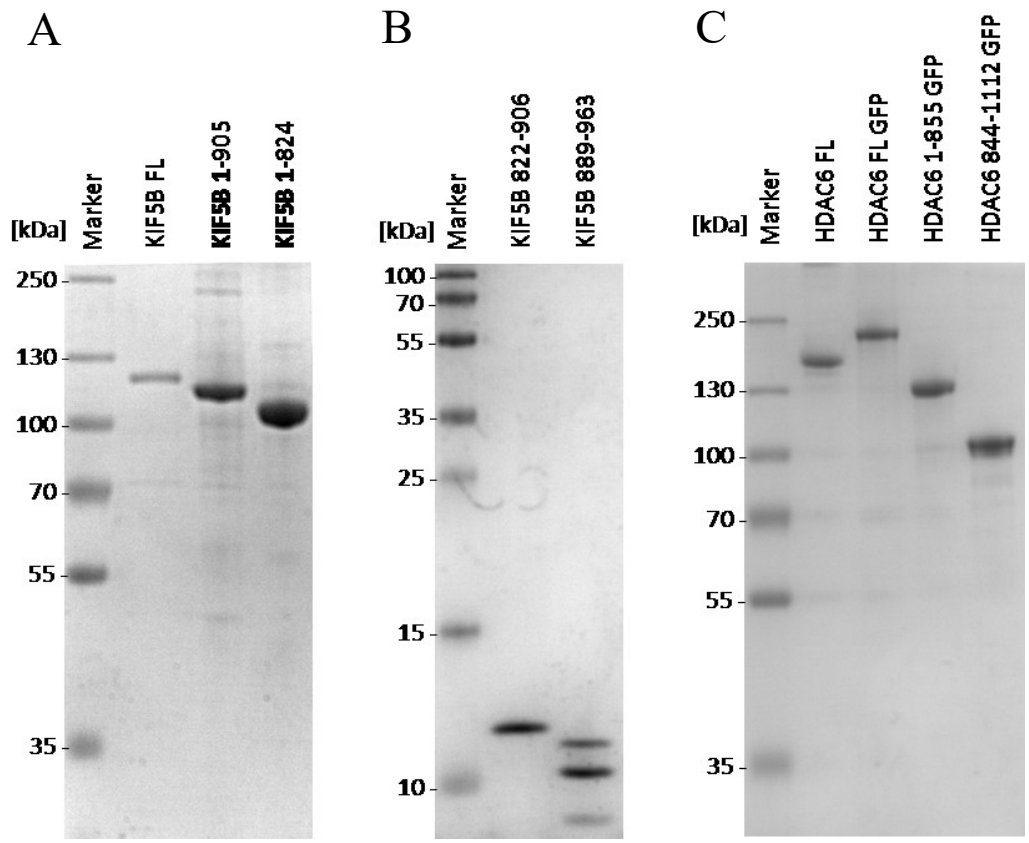

Figure 35 – All purified constructs analyzed by SDS-PAGE

***A** N-terminal KIF5B constructs KIF5B FL (110kDa), KIF5B 1-905 (104 kDa) and KIF5B 1-824 (94 kDa) in a 10% polyacrylamide gel, **B** C-terminal KIF5B constructs KIF5B 822-906 (10 kDa) and partially cleaved KIF5B 889-963 (8 kDa) on a 17.5% polyacrylamide gel, **C** HDAC6 constructs HDAC6 FL (131 kDa), HDAC6 FL-GFP (166 kDa), HDAC6 1-855-GFP (130 kDa) and HDAC6 844-1112-GFP (62 kDa) in a 10% polyacrylamide gel*

4.3. Microscale Thermophoresis (MST)

MST was used to analyze the affinity of HDAC6 and KIF5B using Monolith NT.115 (NanoTemper, Germany). In this technique, the interaction between molecules is monitored through change in fluorescence induced by movement in temperature gradient. The 100nM GFP-labelled HDAC6 full-length (FL) or 1-855 construct were mixed with 2-fold dilution series of KIF5B constructs. The number of measurements was n=2. The GFP-HALO protein and FITC-labelled HDAC8 were used as negative controls.

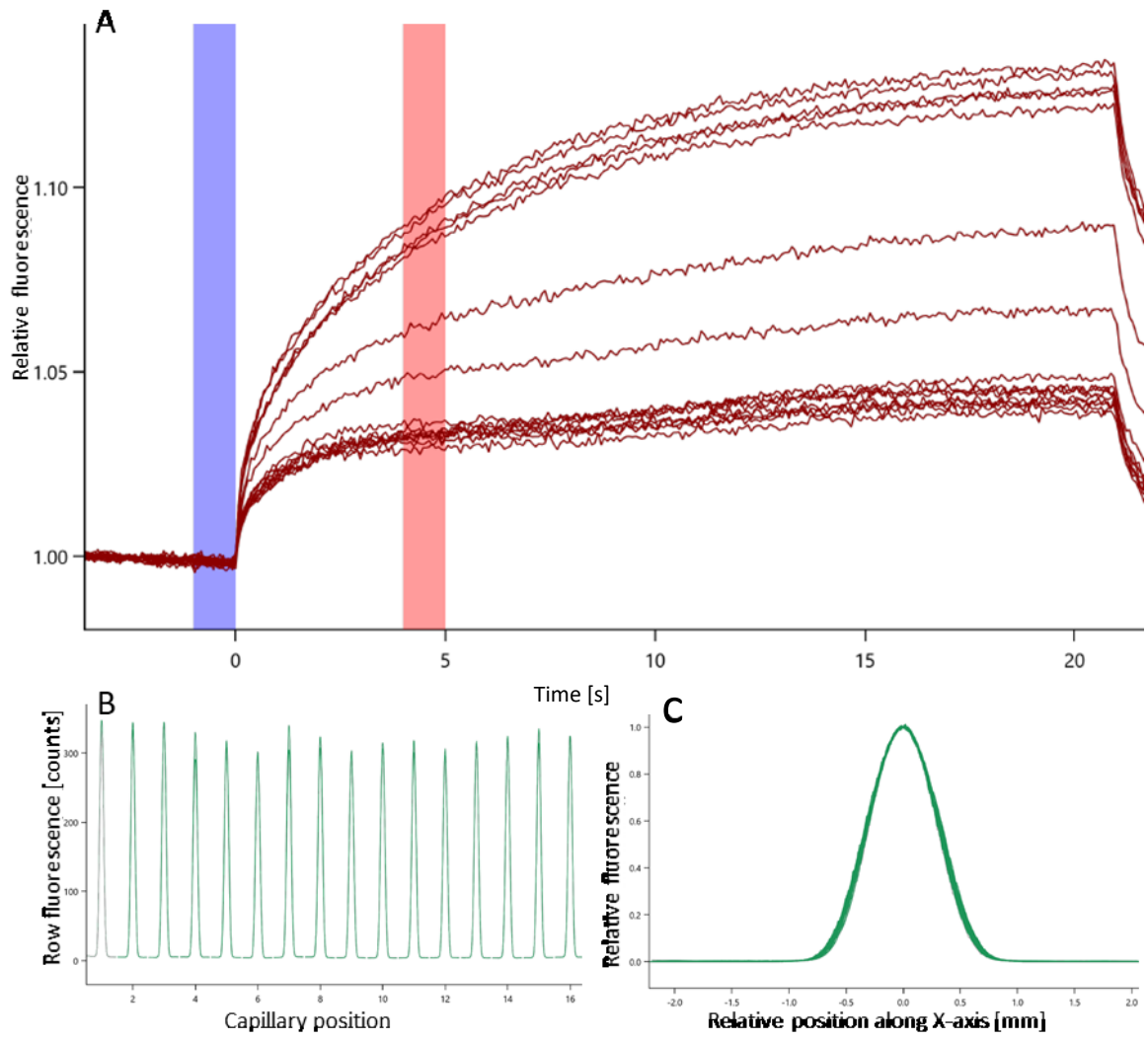

Figure 26 - MST – A representative HDAC6 FL-KIF5B FL experiment

***A** Thermophoresis curves for all concentrations for HDAC6 FL and KIF5B FL, the purple and salmon pink stripes show time point that the thermophoresis results are calculated from. **B** A capillary scan result of the fluorescence level check. **C** A capillary shape scan check to avoid interference with the capillary surface.*

Shapes of thermophoresis curves were inspected to eliminate the possibility of aggregation interference (Figure 26, A). The capillary scan was run before and after every experiment to avoid false positive results caused by different levels fluorescence (Figure 26, B). Interference of non-specific interactions with the capillary surface (Monolith NT.115 Capillaries, NanoTemper, Germany) was monitored by the capillary shape scan (Figure 26, C).

The MST data calculated from the thermophoresis curves were fitted by the [Agonist] vs. response – Variable slope from GraphPad Prism (described in Chapter 1.3). This model was used to determine the half maximal effective concentrations (EC50) of the interaction (Table 3, Figure 27). The response unit

in ‰ of normalized fluorescence (Fnorm) is defined as the ratio between the fluorescence after (F_{hot}) and before (F_{cold}) heating with an infrared laser. The Fnorm is plotted against the concentration of a KIF5B construct. The minimal amplitude of a curve to consider an interaction was 15 ‰ Fnorm.

Table 3 - Table of EC50 values of HDAC6 and KIF5B constructs

HDAC6 construct	KIF5B construct	EC50 [µM]	Amplitude [‰ Fnorm]
HDAC6 FL	KIF5B FL	0.62 ± 0.046	23.3
	KIF5B 1-905	0.35 ± 0.038	56.4
	KIF5B 1-824	~1.11 ± 0.121	43.3
	KIF5B 822-906	~1.91 ± 0.199	36.8
	KIF5B 889-963	No binding	14.9
HDAC6 1-855	KIF5B FL	1.78 ± 0.171	39.2
	KIF5B 1-905	0.32 ± 0.014	88.9
	KIF5B 1-824	No binding	11.4
	KIF5B 822-906	0.93 ± 0.130	24.1
	KIF5B 889-963	No binding, aggregation	

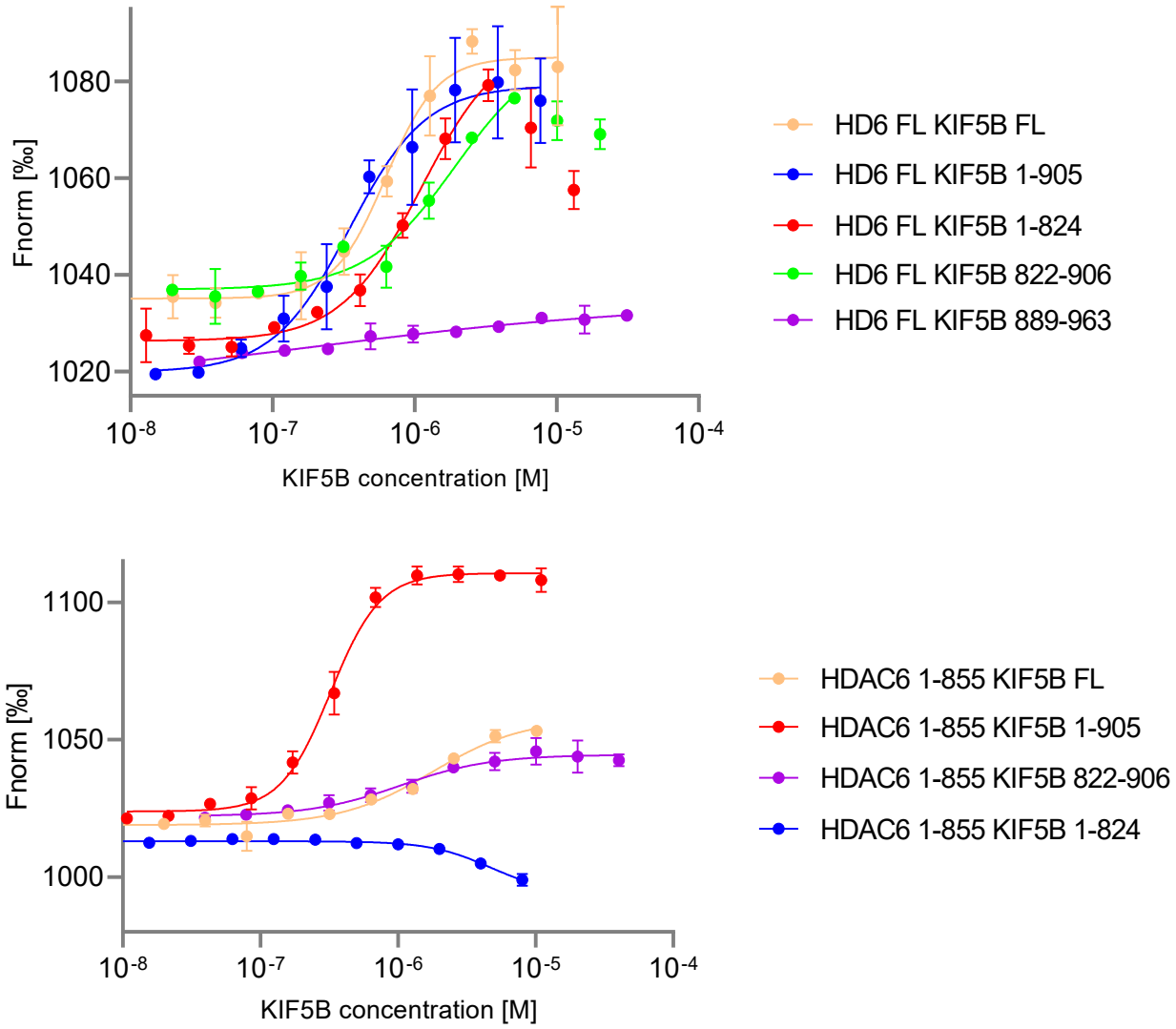

Figure 27 – Binding curves of GFP-labelled HDAC6 FL and HDAC6 1-855 with KIF5B constructs

All KIF5B constructs bind to HDAC6 FL except for KIF5B 889-963. The KIF5B 889-963 construct does not bind to HDAC6 1-855 either. The construct KIF5B 1-824 binds to HDAC6 FL but it does not bind to HDAC6 1-855 even though there is a decrease in fluorescence signal at the two highest concentrations that might be caused by interference. All the other KIF5B constructs interact with both HDAC6 FL and HDAC6 1-855 in high nanomolar range. The highest HDAC6 affinity was observed for the KIF5B 1-905 variant. It is 0.35µM and 0.32µM EC50 for HDAC6 FL and HDAC6 1-855, respectively.

These findings suggest that the tail domain of KIF5B (AA 906-963) does not play an important role in the KIF5B – HDAC6 interaction. Additionally, as the tail is responsible for the autoinhibition, it can be a destabilising or competitive factor in the interaction of KIF5B FL with HDAC6.

In some cases, there is a decrease in a fluorescence signal at high analyte concentrations. This phenomenon has an explanation in binding stoichiometry.(100) At low analyte concentrations, two molecules of HDAC6 binds to one dimer of KIF5B. As the concentration of KIF5B is higher, only one molecule can be bound to the dimer changing the thermophoretic mobility, the decrease in fluorescence signal. It is further discussed below in Chapter 4.

4.4. Structural Analysis

4.4.1. Hydrogen/Deuterium Exchange

HDX experiments were carried out to map the KIF5B/HDAC6 interaction interface in more detail. To this end, H/D exchange rates were first determined for free KIF5B and HDAC6 and next compared with HDX rates of KIF5B/HDAC6 complexes. In the latter case, one of the partners was used in a 4-fold molar excess. The HDX was stopped at four time points (20 s, 2 min, 20, min and 2 h) by mixing with a quencher (pH 2.3) and freezing in liquid nitrogen. After thawing, the samples were immediately injected to LC and analyzed by MS.

4.4.1.1. KIF5B

KIF5B FL was analyzed in a free state as well as using a 4-fold excess of HDAC6 FL. Changes in deuteration of several peptides were found in the coiled-coil region 3 (AA 874-903) (Figure 28). The changes are observed only in the first two time points suggesting a transient character of the interaction. The 2-hour time point may not be relevant because it decreases in some cases. The decrease can be caused by aggregation of a part of one of the interacting partners. Unfortunately, no data were obtained for the KIF5B tail domain as it is unstructured. Unstructured parts are immediately highly deuterated, and changes observed in these regions can be more complicated to interpret (Supplementary Material, Figure 1).

The C-terminal coiled-coil 3 construct KIF5B 822-906 was used for another HDX experiment as it consists of the region probably responsible for interactions with HDAC6. These results corroborate finding for the KIF5B FL as we observed changes in deuteration in the 874-903 region. Additional changes were also observed for the amino acid segment 839-853. In this region, there were only very slight changes observed in the experiment using KIF5B FL. The overall deuteration is higher in case of KIF5B 822-906 and the differences in deuteration between the free molecule and the complex are also higher. These variances can be caused by interference of the other parts of KIF5B FL.

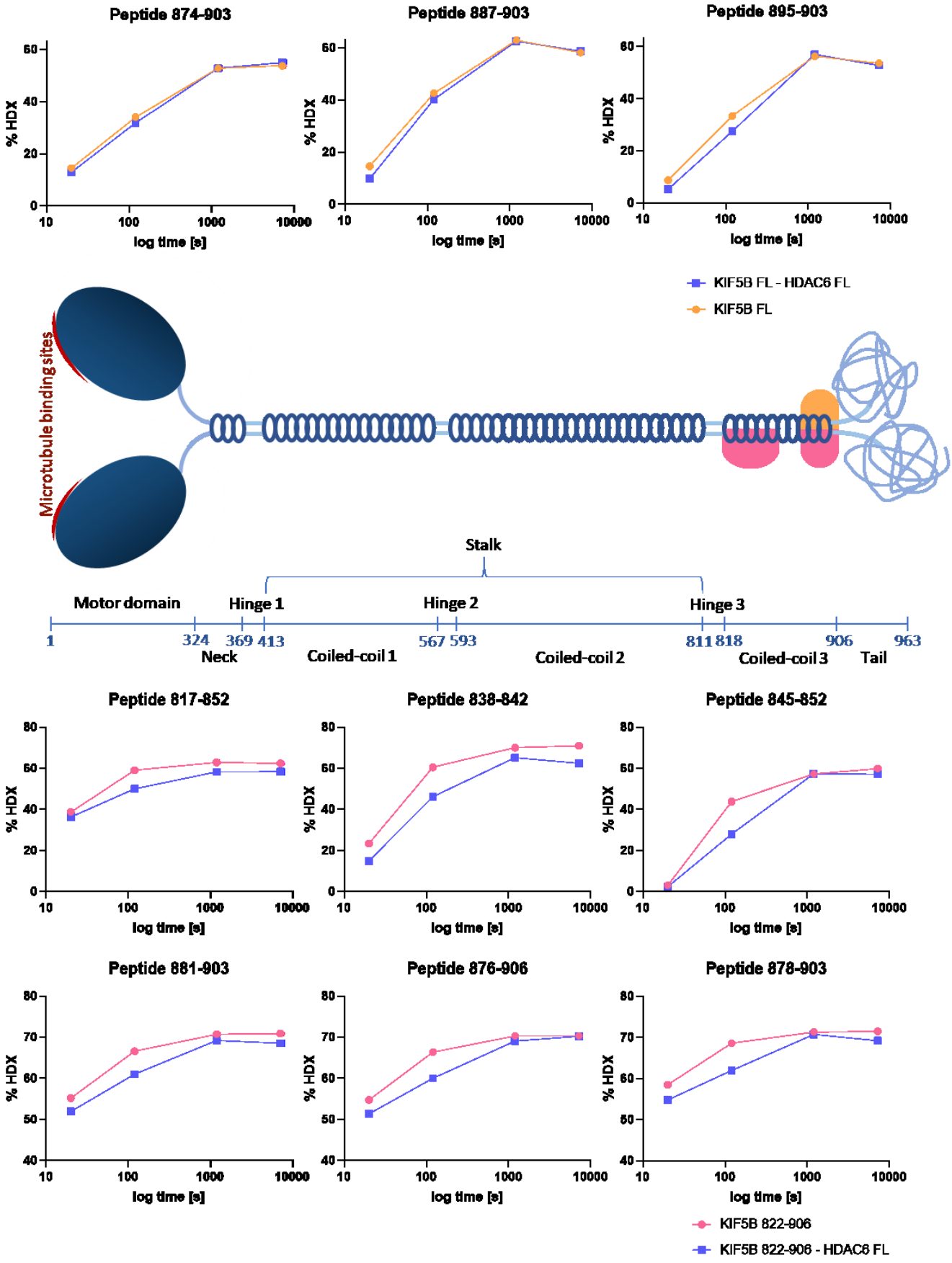

Figure 28 – Deuteration rate changes at KIF5B FL (orange) and KIF5B 822-906 (pink) in complex with HDAC6 FL

4.4.1.2. HDAC6

HDAC6 FL was analyzed in 4-fold excess of KIF5B FL/KIF5B 822-906 and compared with the free state. In the case of interactions with KIF5B FL, changes in deuteration were found in three parts of DD2 (amino acids 496-533, 700-716 and 737-765) (Figure 29). The surface of the first part (amino acids 496-533) is mostly separated from the other two segments. Nevertheless, the two segments (amino acids 700-716 and 737-765 form a continuous patch on the surface of DD2.

In the case of the HDAC6/KIF5B 822-906 complex, the only changes in deuteration were observed in the amino acids 496-533 segment (Figure 30). This result suggests that the other remaining two segments (700-715 and 737-765) likely interact with other parts of KIF5B.

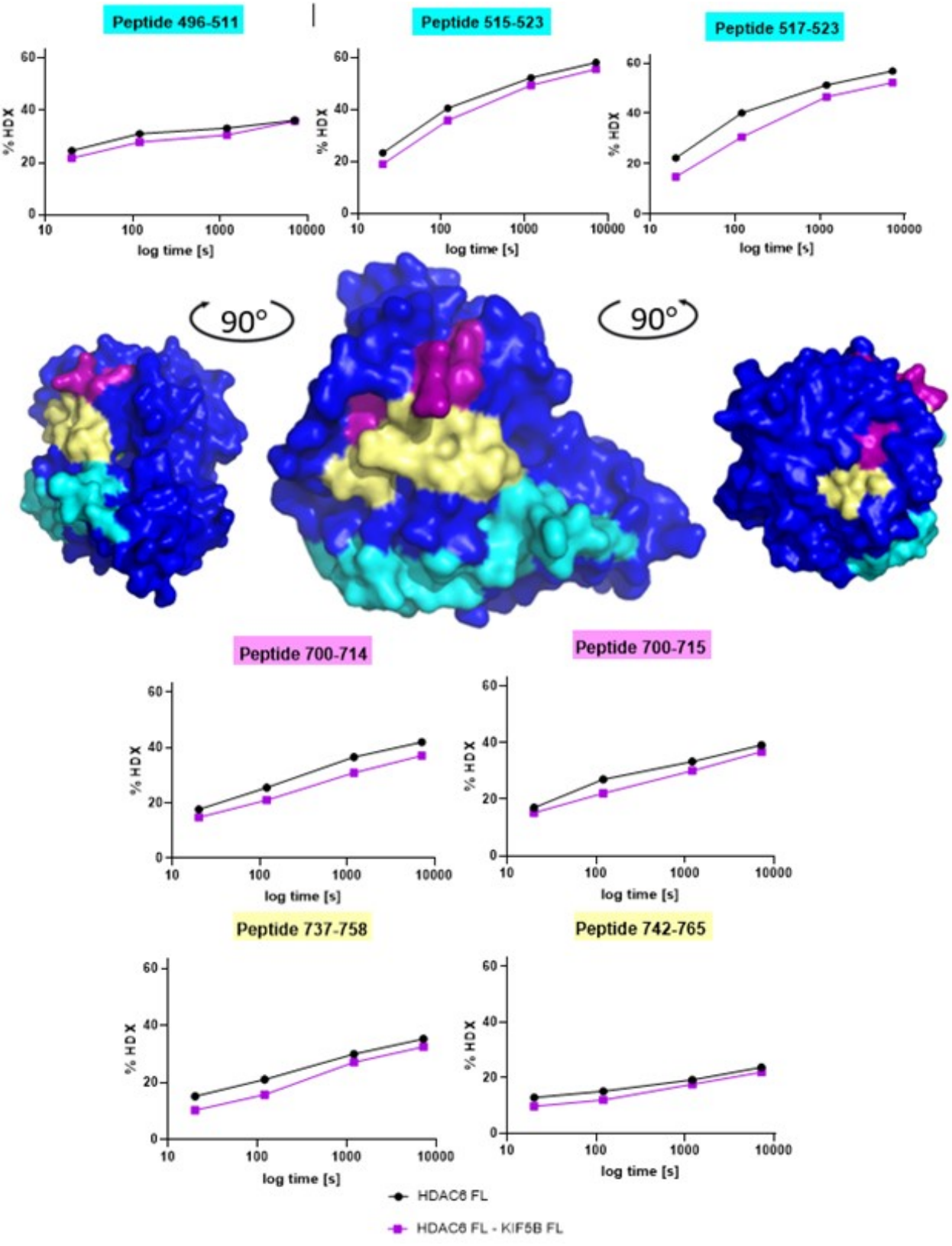

Figure 29 – Deuteration rate changes mapped to the DD2 structure (data from the HDAC6 FL/KIF5B FL complex)

Changes in HDX were observed in the three coloured parts (cyan, purple and yellow) of the DD2 domain. The graphs with headings in corresponding colours show the changes in deuteration rates at representative peptides.

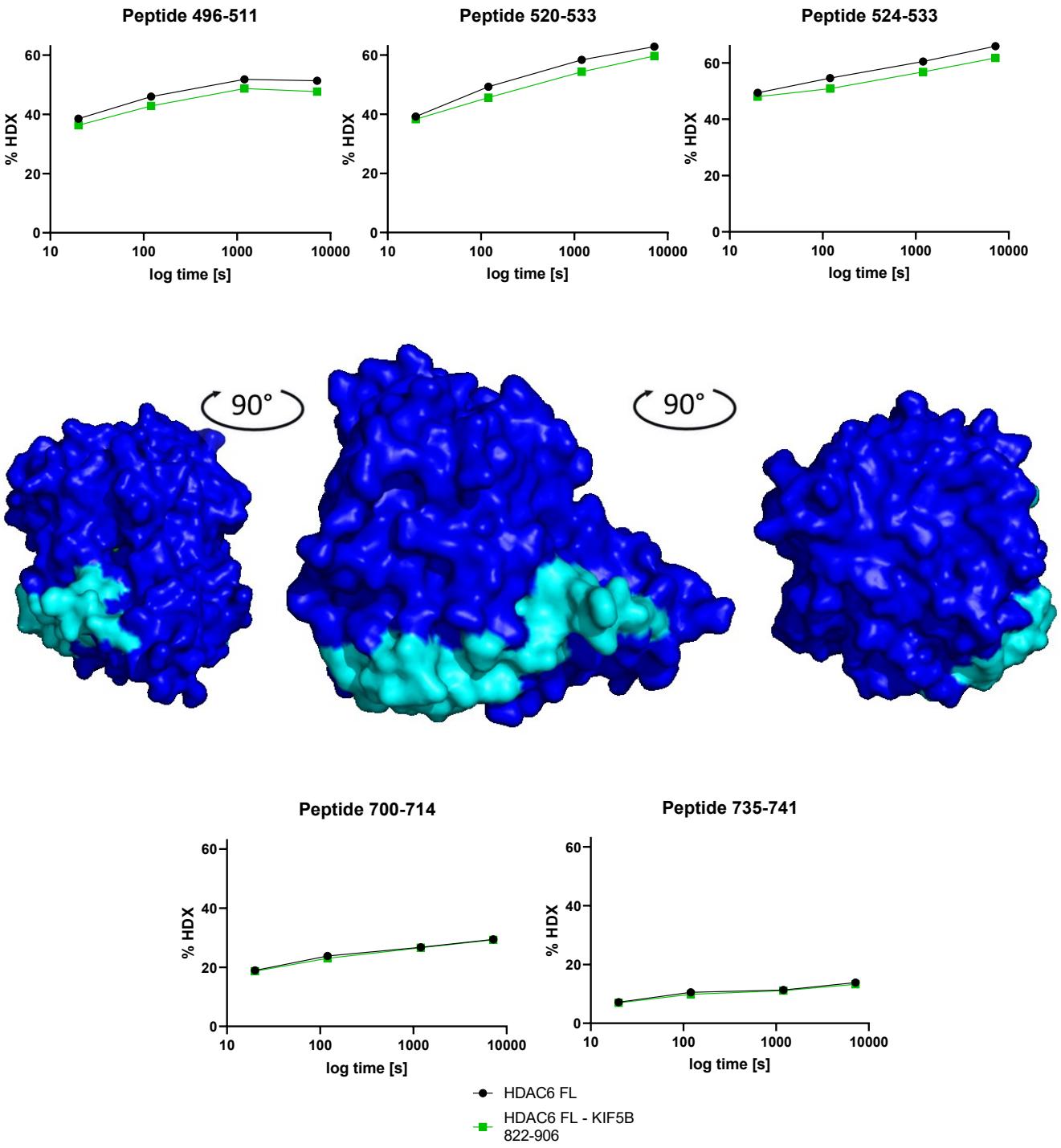

Figure 30 – Deuteration rate changes mapped to the DD2 structure (data from the HDAC6 FL/KIF5B 822-906 complex)

Changes in HDX are coloured in cyan, the corresponding graphs are on the top of the figure. The graphs on the bottom represent no changes in the other two parts of the DD2 where the changes have been observed in case of KIF5B FL (700-716 and 737-765).

4.4.2. Chemical Cross-Linking

HDAC6 FL was cross-linked to KIF5B FL and KIF5B 822-906. The cross-linking reagent used was DSG with the arm-length of 7.5 Å. (101) In the case of HDAC6 FL/KIF5B FL, only a single combination of cross-linked peptides was found in the MS spectra. The cross-link connected KIF5B T195 of the motor domain (Figure 32) and HDAC6 S26 in the N-terminal domain (Figure 31, green). The cross-link between KIF5B 822-906 and HDAC6 FL connected K885 from KIF5B with K849 and K872 from the HDAC6 SE14 domain (Figure 31, purple).

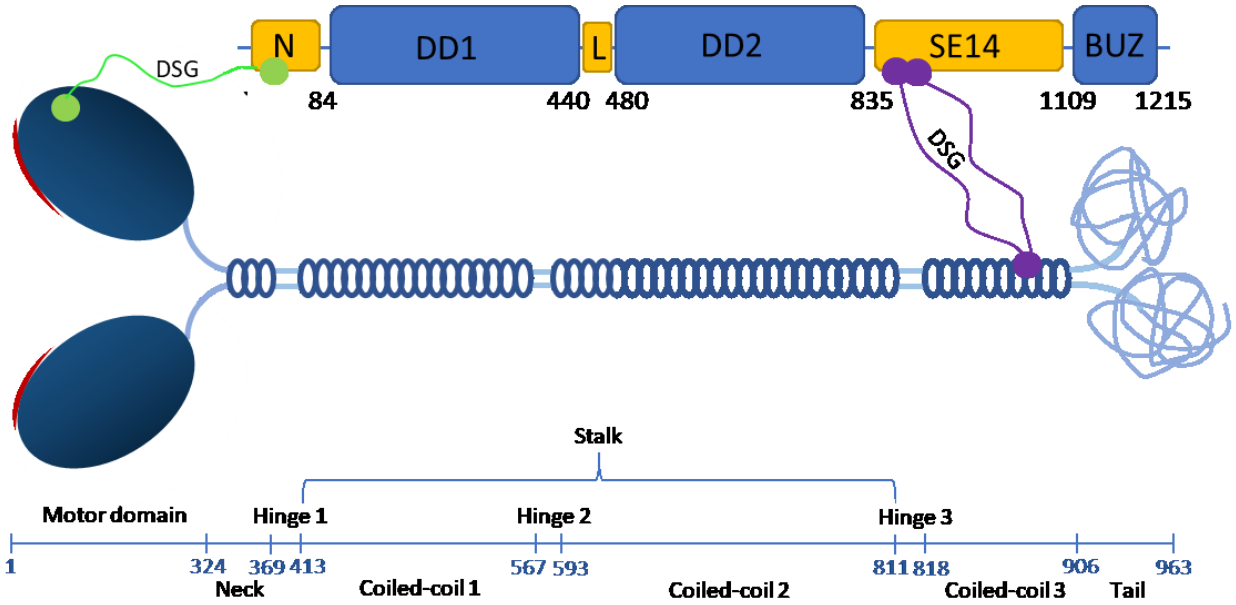

Figure 31 – Schematic picture of HDAC6 and KIF5B structures with DSG cross-links

The green cross-link connects HDAC6 S26 and KIF5B T195, the purple cross-link connects HDAC6 K849 and K872 with KIF5B K885.

The cross-linked amino acids in HDAC6 are from disordered regions that cannot be reliably analyzed by HDX and compared directly with the HDX data. However, in the SE14 domain the cross-links are near the DD2 that interacts with the KIF5B tail domain so that the SE14 domain can interact with the DD2 alongside the KIF5B. Also, if the KIF5B is autoinhibited while interacting with HDAC6, the motor domain can easily interact with the HDAC6 N-terminus.

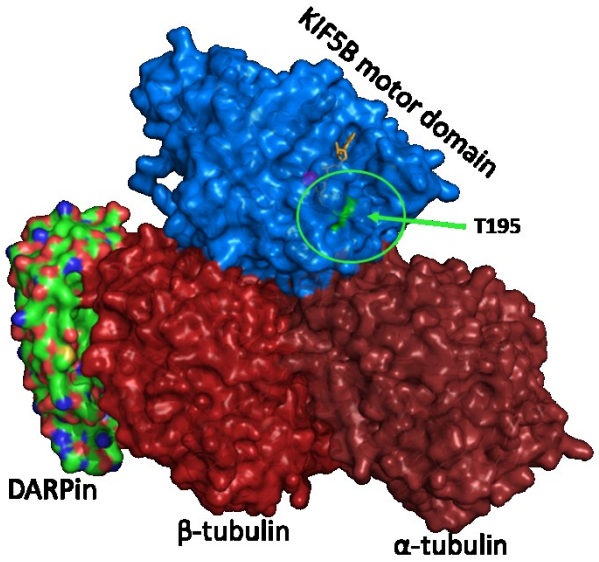

Figure 32 – The KIF5B motor domain in the complex with tubulin with highlighted crosslinked T195 located near the ATP-ase active site

5. Discussion

HDAC6 is a multifunctional protein composed of several domains. It has an important role in regulation of microtubule network dynamics as HDAC6 is a major tubulin deacetylase. (102, 103) It has been shown that inhibition and genetic ablation of HDAC6 affects transport along microtubules, but the exact mechanisms are unknown. The effect can be caused either by the microtubule deacetylation or direct interaction with molecular motors. In this thesis, we provide qualitative and quantitative description of interactions between a kinesin superfamily member KIF5B and HDAC6 as we hypothesized that HDAC6 can be a new factor in the microtubule network dynamics that co-regulates KIF5B activity. To this end, we expressed and purified various constructs of both proteins, tested their affinity and structural aspects of their interactions.

During the purification KIF5B FL, we regularly observed two peaks in SEC chromatogram (Figure 23). Based on the column calibration using globular protein standards (data not shown), molecular weights of protein species in the first and the second peak correspond to ~950 kDa and ~280 kDa, respectively. As the kinesin forms a dimer and a molecular weight of the protomer is 110 kDa, the second peak can be a KIF5B dimer. The first peak might be a tetramer or a dimer in another conformation. When fractions corresponding to individual peaks were reinjected to an analytical SEC column, we observed the identical pattern, i.e. the presence of two separate peaks corresponding to ~950 kDa and ~280 kDa species. Clearly, dynamic equilibrium exists between the two forms of KIF5B. Truncated constructs (KIF5B 1-824 and 1-905) do not form the second peak at all, and they elute at elution volumes similar to the first peak.

In MST runs, we observed a decrease in a normalized fluorescence signal at high analyte concentrations for some KIF5B/HDAC6 pairs (Figure 27, HDAC6 FL/KIF5B 1-824, HDAC6 FL/KIF5B 822-906). As KIF5B is a homodimer it is likely that it has two binding sides for HDAC6 with resulting 1:1 stoichiometry. With the molar excess of HDAC6 at the beginning of titration experiment, each KIF5B homodimer binds two molecules of HDAC6. However, the KIF5B concentration is further increased, one molecule of HDAC6 can bind to a homodimer of KIF5B that results in a change in thermophoretic migration and the decrease of the plateau signal. Apparently, this process has different equilibrium and affinity for every combination of KIF5B/HDAC6 constructs. In some cases, it is absent or very slight and does not interfere with the EC50 calculation. In other cases, such as for HDAC6 FL/KIF5B 1-824 and HDAC6 FL/KIF5B 822-906 pairs, the decrease is quite distinct. The affinity of the second binding event with stoichiometry 1:2 is impossible to calculate from our data as there are only two experimental points in this segment of the binding curve. These experimental points were excluded from the calculation of EC50. The phenomenon was observed for other pairs of molecules, such as human aquaporin 0/calmodulin and *Plasmodium falciparum* AMA1/RON2.(100, 104)

To corroborate the high nanomolar affinity values of KIF5B/HDAC6 binding from our MST measurements, we used surface plasmon resonance (SPR). Unfortunately, however, we have not been so far successful in optimizing SPR runs, even though we tested three types of sensor chips for ligand immobilization. An amino-coupling of KIF5B or HDAC6 on a GLM sensor chip was not possible as the proteins were not stable in buffers suitable for the immobilization (pH lower then pI, pI of HDAC6 is 5.1 and pI od KIF5B is 6.3). On the other hand, the proteins were successfully immobilized on NLC and HTG sensor chips via His-tag and biotin, respectively. As the NLC chip is covered with neutravidine and the HTG chip surface is positively charged, the injected analytes interact non-specifically with these surfaces resulting in a very strong background signal. Even when the background signal from a free line (with no ligand immobilized) and interspot was subtracted, the binding curves were influenced by the non-specific interactions that they cannot be fitted to calculate the affinities (Figure 33). This technical problem was observed when either HDAC6 or KIF5B constructs were used as analytes. At present, we are in the process of optimization of the SPR conditions. In case of need, other methods such as

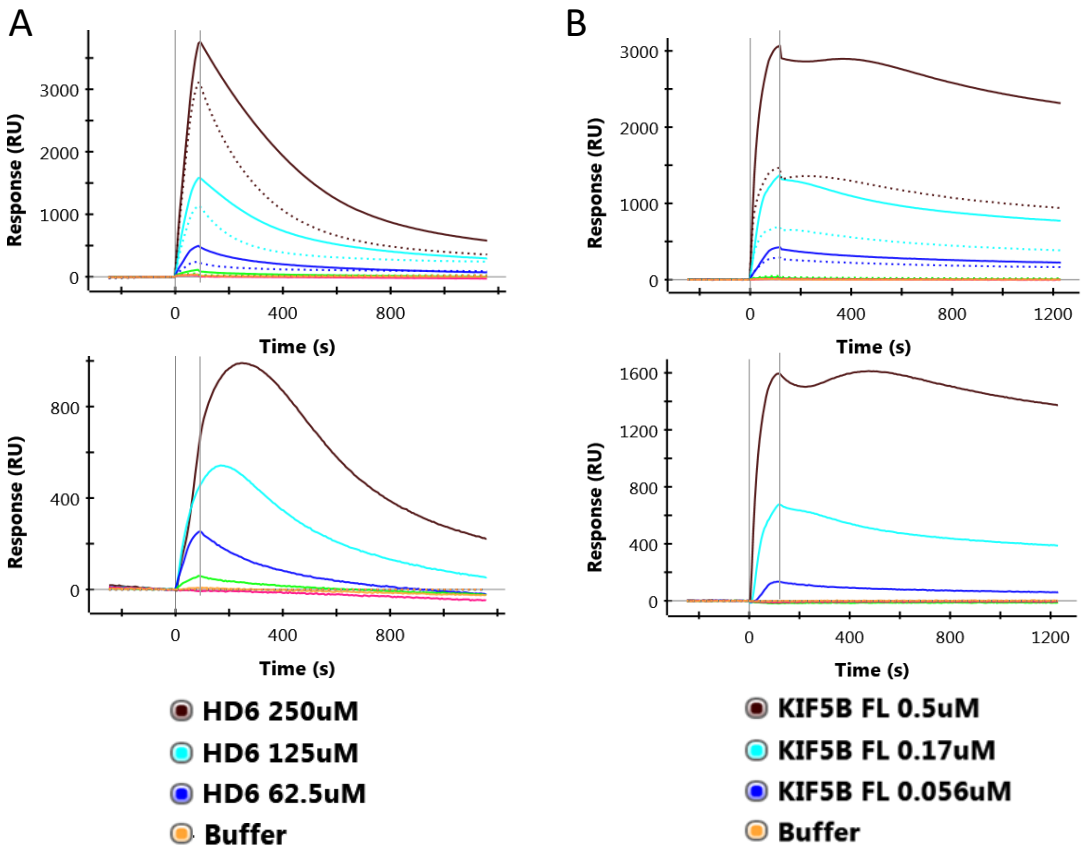

Figure 33 – SPR expreriments using a HTG sensor chip

Top part- Full lines represent signals from spots with immobilized ligand, dotted lines are signal from interspots (derivatized chip surface), bottom part – curves after substraction of the interspot signals. ***A*** *KIF5B FL immobilized on the chip, HDAC6 FL interaction analysis,* ***B*** *HDAC6 FL immobilized on the chip, KIF5B interaction analysis.*

isothermal titration calorimetry or fluorescence anisotropy may be used to corroborate quantitative results from MST.

HDAC6 comprises several domains (Figure 3). The X-ray structure of the full-length human HDAC6 has not been solved. The only structures available are those for the isolated DD2 and BUZ domains. Prediction of the secondary structure shows disordered regions at the N-terminus, the DD1-DD2 linker and the SE14 domain (Figure 5). The presence of unstructured regions is probably the main reason why the full-length HDAC6 cannot be readily crystalized. The flexible SE14 domain spans nearly 300 residues. Theoretical pI of the SE14 domain is 4.0 opening a possibility of ionic interactions with the C-terminal part of KIF5B which has theoretical pI 10.2 (AA 811-963). As we know from the HDX data, KIF5B AA 817-855 and 874-903 interact with HDAC6 and some parts of the interaction can be with SE14.

To test this hypothesis, the SE14 domain was expressed and purified as a fusion protein with GFP (Table 2). The MST binding experiments were done with this construct in the same ways as with HDAC6 FL and HDAC6 1-855, but the protein interacted with the capillary surface and formed aggregates so that it was not possible to measure its affinity for KIF5B. Additionally, the SE14 domain interactions as well as other unstructured proteins is complicated to analyse using HDX because they are immediately highly deuterated (Supplement Materials, Figure 2 and 4).

Furthermore, the MST data show that KIF5B 1-824 does interacts with HDAC6 FL, but it does not interact with HDAC6 1-855. As the BUZ domain is not involved in any KIF5B interactions based on the HDX data, the KIF5B 1-824 construct probably interacts with the SE14 domain (as the SE14 and BUZ domain are not present in the HDAC6 1-855 construct). There are no significant changes in deuteration in the 1-824 segment of KIF5B, so it is likely that the SE14 domain interacts with the hinge 3 part of KIF5B (AA 811-818), which is unstructured and thus highly deuterated. AA 825-963 of KIF5B are implicated in interactions with the DD2 domain of HDAC6. The HDX data support this hypothesis (Figure 30) as HDAC6 FL in the complex with KIF5B 822-906 showed changes in deuteration at AA 496-533 of HDAC6. Changes in deuteration of HDAC6 AA 700-715 and 737-765 can be caused by the interaction with the other parts of KIF5B that were not observed in our HDX data.

When looking at the changes in deuteration of free KIF5B variants and their complexes (Figure 28), they are more distinct changes in case of the construct KIF5B 822-906 then KIF5B FL and some of them are missing. This is probably caused by the protein molecular weight. When analyzing a bigger protein, more peptides are created, trapped and need to be analyzed. This can be a problem, as both KIF5B and HDAC6 are both bigger than 100 kDa and the number of peptides is huge so that the MS signals are weak and more difficult to analyze. We are in process of repeating the experiments to make a statistical analysis.

HDX data show that the construct KIF5B 822-906 (AA 822-852 and 881-903 Figure 28, pink) interacts with DD2 AA 496-523 (Figure 30, cyan). The KIF5B FL/HDAC6 FL complex showed also changes in HDAC6 AA 700-714 and 737-758 (Figure 29, purple and yellow). These additional changes are probably caused by parts of KIF5B other than AA 822-906. Cross-linked K885 of KIF5B with SE14 (K849 and K 872, Figure 31, purple), a part adjacent to DD2, confirms that the KIF5B coiled-coil 3 motif is an important interacting region of KIF5B. This region of KIF5B interacts with an activator, RAN-binding protein 2 as well.(71) If considering autoinhibited conformation of KIF5B, the N-terminus of HDAC6 can be in near proximity of the motor domains explaining thus the cross-link between HDAC6 S26 and KIF5B T195 (Figure 31, green). Overall, HDAC6 interacts with KIF5B in this regulatory region, but it probably does not activate KIF5B on its own. Our results show that the KIF5B/HDAC6 interaction is quite complex as it involves several regions of both proteins. Known regulatory interactions are also complex and several proteins/domains are necessary for kinesin activation.(71) What protein cooperates with HDAC6 in this proposed activation is a subject of further research.

6. Conclusion

- Several KIF5B variants were designed and cloned into expression plasmids
- KIF5B and HDAC6 variants were expressed and purified
- The affinity between KIF5B and HDAC6 was analyzed by MST and the EC50 is in high nanomolar range
- HDAC6-interacting segment of KIF5B is the coiled-coil 3 (amino acids 818-852 and 881-903)
- HDAC6 DD2 domain (amino acids 496-523, 700-715 and 737-758) interacts with KIF5B with possible participation of the SE14 domain

Bibliography

1. Yang XJ, Seto E. The Rpd3/Hda1 family of lysine deacetylases: from bacteria and yeast to mice and men. Nat Rev Mol Cell Biol. 2008;9(3):206-18.
2. Haberland M, Montgomery RL, Olson EN. The many roles of histone deacetylases in development and physiology: implications for disease and therapy. Nat Rev Genet. 2009;10(1):32-42.
3. Li Y, Seto E. HDACs and HDAC Inhibitors in Cancer Development and Therapy. Cold Spring Harb Perspect Med. 2016;6(10).
4. Drazic A, Myklebust LM, Ree R, Arnesen T. The world of protein acetylation. Biochim Biophys Acta. 2016;1864(10):1372-401.
5. Saha RN, Pahan K. HATs and HDACs in neurodegeneration: a tale of disconcerted acetylation homeostasis. Cell Death Differ. 2006;13(4):539-50.
6. Eberharter A, Becker PB. Histone acetylation: a switch between repressive and permissive chromatin. Second in review series on chromatin dynamics. EMBO Rep. 2002;3(3):224-9.
7. Zhang Y, Kwon S, Yamaguchi T, Cubizolles F, Rousseaux S, Kneissel M, et al. Mice Lacking Histone Deacetylase 6 Have Hyperacetylated Tubulin but Are Viable and Develop Normally. Molecular and Cellular Biology. 2008;28(5):1688-701.
8. Szyk A, Deaconescu AM, Spector J, Goodman B, Valenstein ML, Ziolkowska NE, et al. Molecular basis for age-dependent microtubule acetylation by tubulin acetyltransferase. Cell. 2014;157(6):1405-15.
9. Basic Local Alignment Search Tool [18 January 2019]. Available from: https://blast.ncbi.nlm.nih.gov/Blast.cgi.
10. Bertos NR, Gilquin B, Chan GK, Yen TJ, Khochbin S, Yang XJ. Role of the tetradecapeptide repeat domain of human histone deacetylase 6 in cytoplasmic retention. J Biol Chem. 2004;279(46):48246-54.
11. Verdel A, Curtet S, Brocard M-P, Rousseaux S, Lemercier C, Yoshida M, et al. Active maintenance of mHDA2/mHDAC6 histone-deacetylase in the cytoplasm. Current Biology. 2000;10(12):747-9.
12. Hai Y, Christianson DW. Histone deacetylase 6 structure and molecular basis of catalysis and inhibition. Nat Chem Biol. 2016;12(9):741-7.
13. Harding RJ, Ferreira de Freitas R, Collins P, Franzoni I, Ravichandran M, Ouyang H, et al. Small Molecule Antagonists of the Interaction between the Histone Deacetylase 6 Zinc-Finger Domain and Ubiquitin. J Med Chem. 2017;60(21):9090-6.
14. Miyake Y, Keusch JJ, Wang L, Saito M, Hess D, Wang X, et al. Structural insights into HDAC6 tubulin deacetylation and its selective inhibition. Nat Chem Biol. 2016;12(9):748-54.

15. Predict Protein Open [cited 2019 23 January 2019]. Available from: https://open.predictprotein.org.
16. Saji S, Kawakami M, Hayashi S, Yoshida N, Hirose M, Horiguchi S, et al. Significance of HDAC6 regulation via estrogen signaling for cell motility and prognosis in estrogen receptor-positive breast cancer. Oncogene. 2005;24(28):4531-9.
17. Yang W, Liu Y, Gao R, Yu H, Sun T. HDAC6 inhibition induces glioma stem cells differentiation and enhances cellular radiation sensitivity through the SHH/Gli1 signaling pathway. Cancer Lett. 2018;415:164-76.
18. Bitler BG, Wu S, Park PH, Hai Y, Aird KM, Wang Y, et al. ARID1A-mutated ovarian cancers depend on HDAC6 activity. Nat Cell Biol. 2017;19(8):962-73.
19. Santo L, Hideshima T, Kung AL, Tseng JC, Tamang D, Yang M, et al. Preclinical activity, pharmacodynamic, and pharmacokinetic properties of a selective HDAC6 inhibitor, ACY-1215, in combination with bortezomib in multiple myeloma. Blood. 2012;119(11):2579-89.
20. Lee YS, Lim KH, Guo X, Kawaguchi Y, Gao Y, Barrientos T, et al. The cytoplasmic deacetylase HDAC6 is required for efficient oncogenic tumorigenesis. Cancer Res. 2008;68(18):7561-9.
21. Batchu SN, Brijmohan AS, Advani A. The therapeutic hope for HDAC6 inhibitors in malignancy and chronic disease. Clin Sci (Lond). 2016;130(12):987-1003.
22. Rodriguez-Gonzalez A, Lin T, Ikeda AK, Simms-Waldrip T, Fu C, Sakamoto KM. Role of the aggresome pathway in cancer: targeting histone deacetylase 6-dependent protein degradation. Cancer Res. 2008;68(8):2557-60.
23. Hideshima T, Bradner JE, Wong J, Chauhan D, Richardson P, Schreiber SL, et al. Small-molecule inhibition of proteasome and aggresome function induces synergistic antitumor activity in multiple myeloma. Proc Natl Acad Sci U S A. 2005;102(24):8567-72.
24. Thomas S, Munster PN. Histone deacetylase inhibitor induced modulation of anti-estrogen therapy. Cancer Lett. 2009;280(2):184-91.
25. Bennett EJ, Bence NF, Jayakumar R, Kopito RR. Global impairment of the ubiquitin-proteasome system by nuclear or cytoplasmic protein aggregates precedes inclusion body formation. Mol Cell. 2005;17(3):351-65.
26. Ciechanover A, Brundin P. The Ubiquitin Proteasome System in Neurodegenerative Diseases. Neuron. 2003;40(2):427-46.
27. Kawaguchi Y, Kovacs JJ, McLaurin A, Vance JM, Ito A, Yao T-P. The Deacetylase HDAC6 Regulates Aggresome Formation and Cell Viability in Response to Misfolded Protein Stress. Cell. 2003;115(6):727-38.
28. Seigneurin-Berny D, Verdel A, Curtet S, Lemercier C, Garin J, Rousseaux S, et al. Identification of Components of the Murine Histone Deacetylase 6 Complex: Link between Acetylation and Ubiquitination Signaling Pathways. Molecular and Cellular Biology. 2001;21(23):8035-44.

29. Wong E, Cuervo AM. Autophagy gone awry in neurodegenerative diseases. Nat Neurosci. 2010;13(7):805-11.
30. Watabe M, Nakaki T. Protein kinase CK2 regulates the formation and clearance of aggresomes in response to stress. J Cell Sci. 2011;124(Pt 9):1519-32.
31. Pugacheva EN, Jablonski SA, Hartman TR, Henske EP, Golemis EA. HEF1-dependent Aurora A activation induces disassembly of the primary cilium. Cell. 2007;129(7):1351-63.
32. Lafarga V, Aymerich I, Tapia O, Mayor F, Jr., Penela P. A novel GRK2/HDAC6 interaction modulates cell spreading and motility. EMBO J. 2012;31(4):856-69.
33. Simoes-Pires C, Zwick V, Nurisso A, Schenker E, Carrupt PA, Cuendet M. HDAC6 as a target for neurodegenerative diseases: what makes it different from the other HDACs? Mol Neurodegener. 2013;8:7.
34. Chen S, Owens GC, Makarenkova H, Edelman DB. HDAC6 regulates mitochondrial transport in hippocampal neurons. PLoS One. 2010;5(5):e10848.
35. Hubbert C, Guardiola A, Shao R, Kawaguchi Y, Ito A, Nixon A, et al. HDAC6 is a microtubule-associated deacetylase. Nature. 2002;417(6887):455-8.
36. Zhang Y, Li N, Caron C, Matthias G, Hess D, Khochbin S, et al. HDAC-6 interacts with and deacetylates tubulin and microtubules in vivo. EMBO J. 2003;22(5):1168-79.
37. Leroy K, Yilmaz Z, Brion JP. Increased level of active GSK-3beta in Alzheimer's disease and accumulation in argyrophilic grains and in neurones at different stages of neurofibrillary degeneration. Neuropathol Appl Neurobiol. 2007;33(1):43-55.
38. Reed NA, Cai D, Blasius TL, Jih GT, Meyhofer E, Gaertig J, et al. Microtubule Acetylation Promotes Kinesin-1 Binding and Transport. Current Biology. 2006;16(21):2166-72.
39. Bulinski JC. Microtubule modification: acetylation speeds anterograde traffic flow. Curr Biol. 2007;17(1):R18-20.
40. Dompierre JP, Godin JD, Charrin BC, Cordelieres FP, King SJ, Humbert S, et al. Histone deacetylase 6 inhibition compensates for the transport deficit in Huntington's disease by increasing tubulin acetylation. J Neurosci. 2007;27(13):3571-83.
41. Nam W, Epureanu BI. Effects of Obstacles on the Dynamics of Kinesins, Including Velocity and Run Length, Predicted by a Model of Two Dimensional Motion. PLoS One. 2016;11(1):e0147676.
42. Jamison DK, Driver JW, Rogers AR, Constantinou PE, Diehl MR. Two kinesins transport cargo primarily via the action of one motor: implications for intracellular transport. Biophys J. 2010;99(9):2967-77.
43. Hirokawa N. Kinesin and Dynein Superfamily Proteins and the Mechanism of Organelle Transport. Science. 1998;279(5350):519-26.
44. Kaan HY, Hackney DD, Kozielski F. The structure of the kinesin-1 motor-tail complex reveals the mechanism of autoinhibition. Science. 2011;333(6044):883-5.

45. Cai D, Hoppe AD, Swanson JA, Verhey KJ. Kinesin-1 structural organization and conformational changes revealed by FRET stoichiometry in live cells. J Cell Biol. 2007;176(1):51-63.
46. Hancock WO, Howard J. Kinesin's processivity results from mechanical and chemical coordination between the ATP hydrolysis cycles of the two motor domains. Proceedings of the National Academy of Sciences. 1999;96(23):13147-52.
47. Shastry S, Hancock WO. Interhead tension determines processivity across diverse N-terminal kinesins. Proc Natl Acad Sci U S A. 2011;108(39):16253-8.
48. Uemura S, Ishiwata S. Loading direction regulates the affinity of ADP for kinesin. Nat Struct Biol. 2003;10(4):308-11.
49. Asenjo AB, Sosa H. A mobile kinesin-head intermediate during the ATP-waiting state. Proc Natl Acad Sci U S A. 2009;106(14):5657-62.
50. Mickolajczyk KJ, Deffenbaugh NC, Arroyo JO, Andrecka J, Kukura P, Hancock WO. Kinetics of nucleotide-dependent structural transitions in the kinesin-1 hydrolysis cycle. Proc Natl Acad Sci U S A. 2015;112(52):E7186-93.
51. Hancock WO. The Kinesin-1 Chemomechanical Cycle: Stepping Toward a Consensus. Biophys J. 2016;110(6):1216-25.
52. Sindelar CV. A seesaw model for intermolecular gating in the kinesin motor protein. Biophysical Reviews. 2011;3(2).
53. Sindelar CV, Downing KH. An atomic-level mechanism for activation of the kinesin molecular motors. Proceedings of the National Academy of Sciences. 2010;107(9):4111-6.
54. Shang Z, Zhou K, Xu C, Csencsits R, Cochran JC, Sindelar CV. High-resolution structures of kinesin on microtubules provide a basis for nucleotide-gated force-generation. Elife. 2014;3:e04686.
55. Sindelar CV, Budny MJ, Rice S, Naber N, Fletterick R, Cooke R. Two conformations in the human kinesin power stroke defined by X-ray crystallography and EPR spectroscopy. Nat Struct Biol. 2002;9(11):844-8.
56. Hoeprich GJ, Thompson AR, McVicker DP, Hancock WO, Berger CL. Kinesin's neck-linker determines its ability to navigate obstacles on the microtubule surface. Biophys J. 2014;106(8):1691-700.
57. Hirokawa N, Takemura R. Molecular motors and mechanisms of directional transport in neurons. Nat Rev Neurosci. 2005;6(3):201-14.
58. Gindhart JG. Towards an understanding of kinesin-1 dependent transport pathways through the study of protein-protein interactions. Brief Funct Genomic Proteomic. 2006;5(1):74-86.
59. Vale RD, Fletterick RJ. The design plan of kinesin motors. Annu Rev Cell Dev Biol. 1997;13:745-77.

60. Skoufias DA, Cole DG, Wedaman KP, Scholey JM. The Carboxyl-Terminal Domain of Kinesin Heavy-Chain Is Important for Membrane-Binding. Journal of Biological Chemistry. 1994;269(2):1477-85.
61. Toyoshima I, Yu H, Steuer ER, Sheetz MP. Kinectin, a major kinesin-binding protein on ER. J Cell Biol. 1992;118(5):1121-31.
62. Ong LL, Lim AP, Er CP, Kuznetsov SA, Yu H. Kinectin-kinesin binding domains and their effects on organelle motility. J Biol Chem. 2000;275(42):32854-60.
63. Blasius TL, Cai D, Jih GT, Toret CP, Verhey KJ. Two binding partners cooperate to activate the molecular motor Kinesin-1. J Cell Biol. 2007;176(1):11-7.
64. Horiuchi D, Collins CA, Bhat P, Barkus RV, Diantonio A, Saxton WM. Control of a kinesin-cargo linkage mechanism by JNK pathway kinases. Curr Biol. 2007;17(15):1313-7.
65. Gindhart JG, Chen J, Faulkner M, Gandhi R, Doerner K, Wisniewski T, et al. The kinesin-associated protein UNC-76 is required for axonal transport in the Drosophila nervous system. Mol Biol Cell. 2003;14(8):3356-65.
66. Kuroda S, Nakagawa N, Tokunaga C, Tatematsu K, Tanizawa K. Mammalian Homologue of the Caenorhabditis elegans UNC-76 Protein Involved in Axonal Outgrowth Is a Protein Kinase C ζ–interacting Protein. J Cell Biol. 1999:403-11.
67. Lee S, Walker CL, Karten B, Kuny SL, Tennese AA, O'Neill MA, et al. Essential role for the Prader-Willi syndrome protein necdin in axonal outgrowth. Hum Mol Genet. 2005;14(5):627-37.
68. Miyoshi K, Honda A, Baba K, Taniguchi M, Oono K, Fujita T, et al. Disrupted-In-Schizophrenia 1, a candidate gene for schizophrenia, participates in neurite outgrowth. Mol Psychiatry. 2003;8(7):685-94.
69. Okumura F, Hatakeyama S, Matsumoto M, Kamura T, Nakayama KI. Functional regulation of FEZ1 by the U-box-type ubiquitin ligase E4B contributes to neuritogenesis. J Biol Chem. 2004;279(51):53533-43.
70. Suzuki T, Okada Y, Semba S, Orba Y, Yamanouchi S, Endo S, et al. Identification of FEZ1 as a protein that interacts with JC virus agnoprotein and microtubules: role of agnoprotein-induced dissociation of FEZ1 from microtubules in viral propagation. J Biol Chem. 2005;280(26):24948-56.
71. Cho K-i, Yi H, Desai R, Hand AR, Haas AL, Ferreira PA. RANBP2 is an allosteric activator of the conventional kinesin-1 motor protein, KIF5B, in a minimal cell-free system. EMBO reports. 2009;10(5):480-6.
72. Neilson DE, Adams MD, Orr CM, Schelling DK, Eiben RM, Kerr DS, et al. Infection-triggered familial or recurrent cases of acute necrotizing encephalopathy caused by mutations in a component of the nuclear pore, RANBP2. Am J Hum Genet. 2009;84(1):44-51.

73. Cho KI, Cai Y, Yi H, Yeh A, Aslanukov A, Ferreira PA. Association of the kinesin-binding domain of RanBP2 to KIF5B and KIF5C determines mitochondria localization and function. Traffic. 2007;8(12):1722-35.
74. Tekotte H, Davis I. Intracellular mRNA localization: motors move messages. Trends in Genetics. 2002;18(12):636-42.
75. Huang YS, Carson JH, Barbarese E, Richter JD. Facilitation of dendritic mRNA transport by CPEB. Genes Dev. 2003;17(5):638-53.
76. Ling SC, Fahrner PS, Greenough WT, Gelfand VI. Transport of Drosophila fragile X mental retardation protein-containing ribonucleoprotein granules by kinesin-1 and cytoplasmic dynein. Proc Natl Acad Sci U S A. 2004;101(50):17428-33.
77. Palacios IM. Kinesin light chain-independent function of the Kinesin heavy chain in cytoplasmic streaming and posterior localisation in the Drosophila oocyte. Development. 2002;129(23):5473-85.
78. Bladt F, Tafuri A, Gelkop S, Langille L, Pawson T. Epidermolysis bullosa and embryonic lethality in mice lacking the multi-PDZ domain protein GRIP1. Proc Natl Acad Sci U S A. 2002;99(10):6816-21.
79. Hoogenraad CC, Milstein AD, Ethell IM, Henkemeyer M, Sheng M. GRIP1 controls dendrite morphogenesis by regulating EphB receptor trafficking. Nat Neurosci. 2005;8(7):906-15.
80. Berggard T, Linse S, James P. Methods for the detection and analysis of protein-protein interactions. Proteomics. 2007;7(16):2833-42.
81. Braun P, Gingras AC. History of protein-protein interactions: from egg-white to complex networks. Proteomics. 2012;12(10):1478-98.
82. Rao VS, Srinivas K, Sujini GN, Kumar GN. Protein-protein interaction detection: methods and analysis. Int J Proteomics. 2014;2014:147648.
83. Jones S, Thornton JM. Principles of protein-protein interactions. Proceedings of the National Academy of Sciences. 1996;93(1):13-20.
84. Vaynberg J, Fukuda T, Chen K, Vinogradova O, Velyvis A, Tu Y, et al. Structure of an ultraweak protein-protein complex and its crucial role in regulation of cell morphology and motility. Mol Cell. 2005;17(4):513-23.
85. Nooren IM, Thornton JM. Diversity of protein-protein interactions. EMBO J. 2003;22(14):3486-92.
86. Sheinerman F. Electrostatic aspects of protein–protein interactions. Current Opinion in Structural Biology. 2000;10(2):153-9.
87. Conte LL, Chothia C, Janin J. The atomic structure of protein-protein recognition sites 1 1Edited by A. R. Fersht. Journal of Molecular Biology. 1999;285(5):2177-98.
88. Tompa P, Fuxreiter M. Fuzzy complexes: polymorphism and structural disorder in protein-protein interactions. Trends Biochem Sci. 2008;33(1):2-8.

89. Weiss JN. The Hill equation revisited: uses and misuses. The FASEB Journal. 1997;11(11):835-41.
90. Jerabek-Willemsen M, André T, Wanner R, Roth HM, Duhr S, Baaske P, et al. MicroScale Thermophoresis: Interaction analysis and beyond. Journal of Molecular Structure. 2014;1077:101-13.
91. Douzi B. Protein-Protein Interactions: Surface Plasmon Resonance. Methods Mol Biol. 2017;1615:257-75.
92. Sinz A. Chemical cross-linking and mass spectrometry to map three-dimensional protein structures and protein-protein interactions. Mass Spectrom Rev. 2006;25(4):663-82.
93. Green NS, Reisler E, Houk KN. Quantitative evaluation of the lengths of homobifunctional protein cross-linking reagents used as molecular rulers. Protein Sci. 2001;10(7):1293-304.
94. Oganesyan I, Lento C, Wilson DJ. Contemporary hydrogen deuterium exchange mass spectrometry. Methods. 2018;144:27-42.
95. Zhang Z, Smith DL. Determination of amide hydrogen exchange by mass spectrometry: a new tool for protein structure elucidation. Protein Sci. 1993;2(4):522-31.
96. Benson EE, Linderstrøm-Lang K. Deuterium exchange between myoglobin and water. Biochimica et Biophysica Acta. 1959;32:579-81.
97. Gallagher ES, Hudgens JW. Mapping Protein-Ligand Interactions with Proteolytic Fragmentation, Hydrogen/Deuterium Exchange-Mass Spectrometry. Methods Enzymol. 2016;566:357-404.
98. Skultetyova L, Ustinova K, Kutil Z, Novakova Z, Pavlicek J, Mikesova J, et al. Human histone deacetylase 6 shows strong preference for tubulin dimers over assembled microtubules. Sci Rep. 2017;7(1):11547.
99. Young MM, Tang N, Hempel JC, Oshiro CM, Taylor EW, Kuntz ID, et al. High throughput protein fold identification by using experimental constraints derived from intramolecular cross-links and mass spectrometry. Proc Natl Acad Sci U S A. 2000;97(11):5802-6.
100. Kreida S, Roche JV, Olsson C, Linse S, Tornroth-Horsefield S. Protein-protein interactions in AQP regulation - biophysical characterization of AQP0-CaM and AQP2-LIP5 complex formation. Faraday Discuss. 2018;209(0):35-54.
101. Novak P, Young MM, Schoeniger JS, Kruppa GH. A top-down approach to protein structure studies using chemical cross-linking and Fourier transform mass spectrometry. Eur J Mass Spectrom (Chichester). 2003;9(6):623-31.
102. Gao YS, Hubbert CC, Lu J, Lee YS, Lee JY, Yao TP. Histone deacetylase 6 regulates growth factor-induced actin remodeling and endocytosis. Mol Cell Biol. 2007;27(24):8637-47.
103. Zhang X, Yuan Z, Zhang Y, Yong S, Salas-Burgos A, Koomen J, et al. HDAC6 modulates cell motility by altering the acetylation level of cortactin. Mol Cell. 2007;27(2):197-213.

104. Seidel SA, Dijkman PM, Lea WA, van den Bogaart G, Jerabek-Willemsen M, Lazic A, et al. Microscale thermophoresis quantifies biomolecular interactions under previously challenging conditions. Methods. 2013;59(3):301-15.